Evaporative Heat Transfer Characteristics in a Vertical Channel with Obstructions

N. M. DeGuzman and J. C. Chato

ACRC TR-119 May 1997

For additional information:

Air Conditioning and Refrigeration Center
University of Illinois
Mechanical & Industrial Engineering Dept.
1206 West Green Street
Urbana, IL 61801

(217) 333-3115

Prepared as part of ACRC Project 74
Experimental Investigation of Void Fraction
During Refrigerant Condensation and Evaporation
J. C. Chato and T. A. Newell, Principal Investigators

The Air Conditioning and Refrigeration Center was founded in 1988 with a grant from the estate of Richard W. Kritzer, the founder of Peerless of America Inc. A State of Illinois Technology Challenge Grant helped build the laboratory facilities. The ACRC receives continuing support from the Richard W. Kritzer Endowment and the National Science Foundation. The following organizations have also become sponsors of the Center.

Amana Refrigeration, Inc.
Brazeway, Inc.
Carrier Corporation
Caterpillar, Inc.
Copeland Corporation
Dayton Thermal Products
Delphi Harrison Thermal Systems
Eaton Corporation
Ford Motor Company
Frigidaire Company
General Electric Company
Hydro Aluminum Adrian, Inc.
Indiana Tube Corporation
Lennox International, Inc.
Modine Manufacturing Co.
Peerless of America, Inc.
Redwood Microsystems, Inc.
The Trane Company
Whirlpool Corporation
York International, Inc.

For additional information:

Air Conditioning & Refrigeration Center
Mechanical & Industrial Engineering Dept.
University of Illinois
1206 West Green Street
Urbana IL 61801

217 333 3115

EVAPORATIVE HEAT TRANSFER CHARACTERISTICS IN A VERTICAL CHANNEL WITH OBSTRUCTIONS

Noel Morales de Guzman
Department of Mechanical and Industrial Engineering
University of Illinois at Urbana-Champaign, 1997
John C. Chato, Advisor

ABSTRACT

An experimental study of evaporative heat transfer in a vertical channel with obstructions was conducted. Tests that encompass a range of mass fluxes of 37-220 klb_m/ft^2-s (50-300 kg/m^2-s), heat fluxes of 960-8000 Btu/ft^2-h (3-25 kW/m^2), and inlet qualities of 0.2-0.8 were performed with the working fluid R-134a. For both upward and downward flow, both convective and nucleate boiling were observed. At higher mass fluxes, both flow configurations yield the same heat transfer performance. As mass flux decreases, upward flow has higher heat transfer performance relative to downward flow. The upward flow configuration suppresses nucleate boiling when compared to the downward flow configuration. Upon inspection of the data, there appears to be a discontinuity in heat transfer performance which may be attributed to a flow transition. There are no correlations in the literature that accurately describe the experimental heat transfer data present here.

TABLE OF CONTENTS

PAGE

LIST OF TABLES

LIST OF FIGURES

NOMENCLATURE

A	Constant used in Carey and Mandrusiak correlation based upon single phase tests	
A_s	Internal surface area	
A_{min}	Minimum cross sectional area	
Bo	Boiling number	$=\dfrac{q''}{Gi_{lv}}$
c_{pl}	Liquid specific heat	
Co	Convection number	$=\left(\dfrac{1}{x}-1\right)^{0.8}\left(\dfrac{\rho_v}{\rho_l}\right)^{0.5}$
C_1-C_5	Constants used in Kandlikar	
D	Diameter	
D_o	Reference diameter	
D_h	Hydraulic diameter	
F_{fl}	Fluid dependent parameter used in Kandlikar correlation	
F_{nbf}	Nucleate flow boiling correction factor	
F_{pf}	Nucleate flow boiling pressure correction factor	
F_{tp}	Two-phase flow convection factor	
Fr_{lo}	Liquid Froude number	$=\dfrac{G^2}{\rho_l^2 gD}$
$F(M)$	Flow boiling correction factor	
G	Mass flux	
h	Heat transfer coefficient	
h_{cb}	Single component heat transfer coefficient due to convective boiling	
h_{GO}	Convection coefficient based on total flow as gas	
h_l	Single phase liquid heat transfer coefficient	
h_{LO}	Convection coefficient base on total flow	
h_{mac}	Single component heat transfer coefficient due to macroscopic contribution	
h_{mic}	Single component heat transfer coefficient due to microscopic contribution	

h_{nb}	Single component heat transfer coefficient due to nucleate boiling	
$h_{nb,of}$	Single component heat transfer coefficient due to nucleate boiling under normalized conditions	
h_{tp}	Two-phase heat transfer coefficient	
i_l	Saturated liquid enthalpy	
i_{lv}	Latent heat of vaporation	
$i_{preheater,\ in}$	Enthalpy of refrigerant entering the preheater	
$i_{preheater,\ exit}$	Enthalpy of refrigerant leaving the preheater	
$i_{test\ section,\ in}$	Enthalpy of refrigerant entering the test section	
j_l	Superficial liquid flux	$=\dfrac{G(1-x)}{\rho_l}$
j_v	Superficial vapor flux	$=\dfrac{G}{\rho_v}$
k_l	Liquid thermal conductivity	
$\dot{m}$	Mass flow rate	
N	Variable used in Shah correlation	
Nu	Two-phase Nusselt number	$=\dfrac{h_{tp}D_h}{k_l}$
P	Perimeter	
P_l	Liquid pressure	
P_{sat}	Saturation pressure	
Pr_l	Liquid Prandtl number	$=\dfrac{\mu_l c_{pl}}{k_l}$
q	Heat input	
$q_{preheater}$	Electrical heat input rate to the preaheater	
q''	Heat flux	
q''_{of}	Heat flux at normalized condition, flow boiling	
R_a	Wall roughness	
$R_{a,o}$	Wall roughness at normalized conditions	

Re_l	Liquid only Reynolds number	$= \frac{GD(1-x)}{\mu_l}$
Re_{LO}	Liquid Reynolds number for single phase flow	$= \frac{GD}{\mu_l}$
$\mathrm{Re}_{2\phi}$	Two-phase Reynolds number (Product of liquid only Reynolds number and two-phase multiplier)	
S	Suppression factor	
$\overline{T}_b$	Interpolated values of bulk temperature	
$T_{preheater,\ in}$	Refrigerant temperature at preheater inlet	
$\overline{T}_s$	Average surface temperature at a particular location	
T_{sat}	Saturation temperature	
$T_{test\ section,\ in}$	Refrigerant temperature at test section inlet	
$T_{test\ section,\ ave}$	Average refrigerant temperature in section	
T_w	Wall temperature	
x	Quality	
X_{tt}	Turbulent-Turbulent Lockhart-Martinelli parameter	$= \left(\frac{\rho_v}{\rho_l}\right)^{0.5} \left(\frac{\mu_l}{\mu_v}\right)^{0.15} \left(\frac{1-x}{x}\right)^{0.35}$
ΔT_s	Superheat	
ΔP_s	Change in saturation pressure corresponding to ΔT_s	
$\partial \mathrm{d}_i$	Uncertainty in diameter measurement	
$\partial \mathrm{h}$	Uncertainty in the heat transfer coefficient	
$\partial \mathrm{L}_{HX}$	Uncertainty in the heat transfer length	
$\partial \dot{\mathrm{Q}}_{TS}$	Uncertainty in the heat input to the test section	
$\partial \overline{\mathrm{T}}_b$	Uncertainty in the average bulk fluid temperature	
$\partial \overline{\mathrm{T}}_s$	Uncertainty in the average surface temperature	
$\frac{\partial \mathrm{h}}{\partial \mathrm{d}_i}$	Sensitivity of heat transfer coefficient w.r.t. diameter	

$\frac{\partial h}{\partial L_{HX}}$	Sensitivity of heat transfer coefficient w.r.t. heat transfer length
$\frac{\partial h}{\partial \dot{Q}_{TS}}$	Sensitivity of heat transfer coefficient w.r.t. heat input
$\frac{\partial h}{\partial \overline{T}_b}$	Sensitivity of heat transfer coefficient w.r.t. average surface temperature
$\frac{\partial h}{\partial \overline{T}_s}$	Sensitivity of heat transfer coefficient w.r.t. average bulk fluid temperature
μ_l	Liquid viscosity
ρ_l	Liquid density
ρ_v	Vapor density
σ	Surface tension
Ψ	Multiplier used in Shah and Carey & Mandrusiak correlations
Ψ_{bs}	Bubble suppression multiplier used in Shah correlation
Ψ_{cb}	Convective boiling multiplier used in Shah correlation
Ψ_{nb}	Nucleate boiling multiplier used in Shah correlation

CHAPTER 1
Introduction

Plate type heat exchangers have been used widely in various capacities such as food and chemical processing as well as aerospace and automotive applications. These heat exchangers have functioned primarily under single phase conditions. Recently, the automotive industry has incorporated these plate type heat exchangers into the mobile air-conditioning system, specifically to function as an evaporator. Factors other than the optimization of heat transfer such as cost, packaging, manufacturability, and weight savings has caused this evolution.

Since these plate type heat exchangers can have an infinite array of configurations for refrigerant flow, it is difficult to generalize the refrigerant two-phase flow and heat transfer characteristics. As a starting point, evaporative two-phase flows in round tubes configured vertically will be referenced. Valuable information regarding flow regimes and heat transfer mechanisms for these round tubes have been studied and confirmed by several researchers. The main difference between the plate type and round tube configurations is that the plate type flow passage is non-circular and usually has obstructions to the refrigerant flow. The underlying motivation of this study will be to explore the heat transfer mechanisms of a plate type arrangement.

The flow boiling heat transfer characteristics of R-134a in a single pass, vertical plate type configuration with flow obstructions will be presented. Both upward and downward flow will be tested and compared. Finally, the experimental data will be compared to correlations presented in the literature.

Background information and existing literature will be reviewed in Chapter 2. In Chapter 3, a description of the experimental apparatus will be presented. Chapter 4 will outline the experimental procedure, controlled variables during the experiments, and test matrix used for this investigation. In Chapter 5, the experimental data will be presented with possible explanations for the heat transfer coefficient behavior. Finally, Chapter 6 will summarize the conclusions of this study.

CHAPTER 2
Literature Review

This literature review will present background information necessary for the discussion of this work and the work performed by other investigators. First, flow regimes associated with vertical flow will be reviewed. Next, a presentation of heat transfer coefficient correlations for vertical evaporative two-phase flow in round tubes will be given. Finally, work done by other investigators in the area of evaporation for plate type geometries will be discussed.

2.1 Flow Regimes in Vertical Two-Phase Flow

The heat transfer coefficient is greatly influenced by the flow regime present during two-phase flow. Therefore, identifying and characterizing the various vertical flow regimes is important when trying to decipher heat transfer coefficient trends.

In the beginning, subcooled liquid gains sensible heat and causes a rise in fluid temperature. Once the evaporation process begins, the fluid gains latent heat which results in constant fluid temperature with phase change. At the very low qualities, the encountered flow regime is called bubbly flow which can be distinguished by small discrete bubbles of vapor which are dispersed in the liquid. As the fluid gains more heat, a transition from bubbly flow to slug flow occurs. Slug flow can be characterized when the bubble size increases to the point where it occupies most of the cross section of the channel. Depending upon the flow conditions, there may be a transition from bubbly flow to churn flow. If such conditions exist, churn flow occurs when the vapor shear on the liquid-vapor interface balances the pressure gradient and the downward gravitational force in the liquid film. When this balance occurs, the vapor flows continuously upward but liquid flow instabilities causes liquid upward and downward motions. These three described flow regimes usually occur at very low mass flows and/or low qualities. The test parameters of the work presented and similar work by other investigators usually do not experience such flow regimes.

The flow regimes that are most frequently observed in circular tubes due to the test conditions used in this study are annular-wispy and annular flow. In the annular flow regime, which usually occurs at the higher qualities, the liquid flow becomes completely turbulent and strong Reynold stresses and shear tend to distribute the liquid evenly around the perimeter [Carey, 1992]. At intermediate qualities, the annular-wispy flow regime which is very similar to the annular flow might be observed. In annular-wispy flow, a uniform liquid film flows along the perimeter of the channel with some "wisps" of entrained liquid flowing in the vapor core.

At the highest qualities, the vapor velocities are very high which causes waves to form at the liquid-vapor interface. These interfacial waves form droplets that are entrained in the vapor core until the liquid layer disappears which is a form of dry out. This is called mist flow. When the droplets that are entrained are vaporized leaving only vapor, this type of flow is single phase. Figure 2.1 shows a visual representation of each flow regime. Figure 2.2 is a flow regime map proposed by Hewitt & Roberts [1969]. On the flow regime map, the vertical coordinate is the superficial momentum flux of the vapor and the horizontal coordinate is the superficial momentum flux of the liquid. The boundaries of the flow regimes, which should be interpreted as a transition, have been determined by visual observation.

2.2 Heat Transfer Correlations for Vertical Flow in Tubes

To gain a better understanding of heat transfer phenomena in vertical flow, the simplified geometry of round tubes is first investigated since much work has been done in this area. Some of the flow regimes that were observed by other investigators when studying round tubes are similar to those observed during the present work. For the range of mass flow rates ($G > 25$ kg/m^{2}s or 19 klb$_m$/ft^2-hr) and qualities ($x > 0.2$) tested for both round tubes and rectangular channels, the predominant flow regime is liquid film flow (known as annular flow for round tubes). Therefore, evaporation studies in rectangular channel with obstructions are being compared to work done in round tubes.

2.2.1 The Chen Correlation

Chen [1966] proposed expressions that correlate 1,000 sets of data for distilled water, ethylene glycol and aqueous mixtures of ethylene glycol to within a mean error of 15%. His two-phase heat transfer coefficient correlation, h_{tp}, is the sum of a microscopic (nucleate boiling) contribution, h_{mic}, and macroscopic (convective boiling) contribution h_{mac}:

$$h_{tp} = h_{mic} + h_{mac} \tag{2.1}$$

The macroscopic contribution, h_{mac}, is determined by multiplying the single phase heat transfer coefficient, h_l, based upon the Dittus-Boelter equation by a two-phase multiplier, $F(X_{tt})$:

$$h_{mac} = h_l \, F(X_{tt}) \tag{2.2}$$

$$h_l = 0.023\left(\frac{k_l}{D}\right) \mathrm{Re}_l^{0.8} \, \mathrm{Pr}_l^{0.4} \tag{2.3}$$

$$Re_l = \frac{G(1-x)D}{\mu_l} \tag{2.4}$$

The microscopic contribution, h_{mic}, is based upon the Forster and Zuber [1955] relation which takes into account property values, amount of superheat, change in saturation pressure determined by the amount of superheat and a suppression factor:

$$h_{mic} = 0.00122\left[\frac{k_l^{0.79} c_{pl}^{0.45} \rho_l^{0.49}}{\sigma^{0.5} \mu_l^{0.29} i_{lv}^{0.24} \rho_v^{0.24}}\right] \Delta T_s^{0.24} \Delta P_s^{0.75} S(\mathrm{Re}_{2\phi}) \tag{2.5}$$

where,

$$\Delta T_s = T_w - T_{sat}(P_l) \tag{2.6}$$

$$\Delta P_s = P_{sat}(T_w) - P_l \tag{2.7}$$

The $F(X_{tt})$ and $S(\mathrm{Re}_{2\phi})$ functions were originally presented in graphical form, but Collier [1981] proposed empirical relations for the curves:

$$F(X_{tt}) = 1 \quad \text{for } X_{tt}^{-1} \leq 0.1 \tag{2.8}$$

$$F(X_{tt}) = 2.35\left(0.213 + \frac{1}{X_{tt}}\right)^{0.736} \quad \text{for } X_{tt}^{-1} > 0.1 \tag{2.9}$$

$$\mathrm{Re}_{2\phi} = \mathrm{Re}_l\left[F(X_{tt})\right]^{1.25} \tag{2.10}$$

$$S(\mathrm{Re}_{2\phi}) = (1 + 2.56x10^{-6}\,\mathrm{Re}_{2\phi}^{1.17})^{-1} \tag{2.11}$$

2.2.2 The Shah Correlation

Shah [1982] presented equations to fit his earlier graphical presentations that were based upon 780 data sets from 19 independent experimental studies. The evaporating fluids used for the correlation were water, R-11, R-12, R-22, R-113, and cyclohexene. The ratio of two-phase heat transfer coefficient to single-phase heat transfer coefficient, Ψ, is based upon criteria determined by the boiling number, *Bo*, convective number, *Co,* and a Froude number, Fr_{lo}, which does not affect evaporation in vertical tubes. The dimensionless parameters are in the form of:

$$Co = \left(\frac{1}{x} - 1\right)^{0.8}\left(\frac{\rho_v}{\rho_l}\right)^{0.5} \tag{2.12}$$

$$Bo = \frac{q''}{Gh_{lv}} \tag{2.13}$$

Once these dimensionless parameters have been determined, two heat transfer correlations are calculated and the larger of the two is used. The single phase heat transfer coefficient, h_l, the multiplier, Ψ, and the two-phase heat transfer coefficient, h_{tp}, are determined by:

$$h_l = 0.023 \frac{k_l}{D} \mathrm{Re}_l^{0.8} \mathrm{Pr}_l^{0.4} \tag{2.14}$$

$$\Psi = \frac{h_{tp}}{h_l} \tag{2.15}$$

$$\Psi_{cb} = 1.8 N^{-0.8} \tag{2.16}$$

For $N > 1.0$:

$$\Psi_{nb} = 230 Bo^{0.5} \quad \text{for } Bo > 0.3 \times 10^{-4} \tag{2.17}$$

$$\Psi_{nb} = 1 + 46 Bo^{0.5} \quad \text{for } Bo \leq 0.3 \times 10^{-4} \tag{2.18}$$

$$\Psi = \text{the larger of } \Psi_{nb} \text{ and } \Psi_{cb} \tag{2.19}$$

For $N \leq 1.0$:

$$\Psi_{bs} = F Bo^{0.5} \exp(2.74 N^{-0.1}) \quad \text{for } 0.1 < N \leq 1.0 \tag{2.20}$$

$$\Psi_{bs} = F Bo^{0.5} \exp(2.47 N^{-0.15}) \quad \text{for } N \leq 0.1 \tag{2.21}$$

$$F = 14.7 \quad \text{for } Bo \geq 11 \times 10^{-4} \tag{2.22}$$

$$F = 15.43 \quad \text{for } Bo < 11 \times 10^{-4} \tag{2.23}$$

$$\Psi = \text{the larger of } \Psi_{bs} \text{ and } \Psi_{cb} \tag{2.24}$$

where

$$N = Co \quad \text{for vertical flow} \tag{2.25}$$

2.2.3 The Kandlikar Correlation

Kandlikar [1990] proposed a correlation to predict saturated flow boiling heat transfer coefficients inside horizontal and vertical tubes. The work is based upon 5246 data points of refrigerant and water tests from 24 experimental investigators. The correlation has a mean deviation of 15.9 % with water data and 18.8 % with refrigerant data. The correlation utilizes contributions due to nucleate and convective boiling. The convection number, *Co,* determines nucleate or convective boiling as the main mode of heat transfer. After the mode of boiling has been determined, constants for the correlation will suppress one of the contributions leaving the total heat transfer coefficient based upon the dominant boiling mode. The correlation is as follows:

$$\frac{h_{tp}}{h_l} = C_1 Co^{C_2} (25 Fr_{lo})^{C_5} + C_3 Bo^{C_4} F_{fl} \tag{2.26}$$

$$h_l = 0.023\left(\frac{k_l}{D}\right) \mathrm{Re}_l^{0.8}\, \mathrm{Pr}_l^{0.4} \tag{2.27}$$

Constant	*Co*<0.65	*Co*>0.65
C_1	1.1360	0.6683
C_2	-0.9	-0.2
C_3	667.2	1058.0
C_4	0.7	0.7
C_5^*	0.3	0.3

$C_5^* = 0$ for vertical tubes

F_{fl} = fluid dependent parameter

2.2.4 The Steiner and Taborek Correlation

Steiner and Taborek [1992] have taken a more physical approach to correlating vertical, two-phase flow data. This physical approach emphasizes a mechanistic model that accounts for all established principles regarding nucleate and convective boiling. As various fundamental aspects of boiling are refined, they can be incorporated easily into this model which uses an asymptotic correlation scheme to provide a smooth transition from one dominated regime to the other. The correlation is as follows with explanation of the various factors.

$$h_{tp} = \left[(h_{nb})^n + (h_{cb})^n\right]^{\frac{1}{n}} \tag{2.28}$$

where h_{tp} is the two phase heat transfer coefficient, h_{nb} is the nucleate boiling contribution, and h_{cb} is the convective boiling contribution. The nucleate and convective boiling contributions are determined from the following.

$$h_{cb} = h_l F_{tp} \tag{2.29}$$

$$h_l = 0.023 \frac{k_l}{D} \mathrm{Re}_{LO}^{0.8} \mathrm{Pr}_l^{0.4} \tag{2.30}$$

$$\mathrm{Re}_{LO} = \frac{GD}{\mu_l} \tag{2.31}$$

$$F_{tp} = \left(\begin{array}{l} \left[(1-x)^{1.5} + 1.9(x)^{0.6}(1-x)^{0.01}\left(\dfrac{\rho_l}{\rho_v}\right)^{0.35} \right]^{-2.2} \\ + \left\{ \left(\dfrac{\alpha_{GO}}{\alpha_{LO}}\right)(x)^{0.01}\left[1 + 8(1-x)^{0.7}\left(\dfrac{\rho_l}{\rho_v}\right)^{0.67}\right] \right\}^{-2} \end{array} \right)^{-0.5} \tag{2.32}$$

For the convective boiling contribution, h_{cb}, the single phase heat transfer coefficient h_l is calculated with the Dittus-Boelter equation without the quality adjustment (1-x). The convective boiling adjustment factor, F_{tp}, is a function of quality, density ratio, liquid and gas heat transfer coefficients which is valid when the critical quality is greater than 0.5. For the nucleate boiling contribution, h_{nb}, a normalized nucleate boiling heat transfer coefficient based upon normalized conditions, $h_{nb,of}$, is multiplied by an adjustment factor,

F_{nbf}. The nucleate boiling adjustment factor takes into account several factors such as pressure correction, reference heat flux, tube diameter, surface roughness and any residual effects, *F(M)*.

$$h_{nb} = h_{nb,of}F_{nbf} \tag{2.33}$$

$$F_{nbf} = F_{pf}\left[\frac{q''}{q''_{of}}\right]^{nf(pr)}\left[\frac{D}{D_o}\right]^{-0.4}\left[\frac{R_a}{R_{a,o}}\right]^{0.133} F(M) \tag{2.34}$$

This correlation was developed from 13,000 data points from several fluids. When comparing this correlation to others, this one seems to provide the highest accuracy with a mean deviation of less than 20%.

2.3 Heat Transfer in Plate Type Geometries

Plate type geometries have become popular because of their use in compact heat exchangers. There has been relatively little work done in this area due to the infinite configurations an enhanced plate geometry may possess and the complexity of two phase flows in such geometries. In the following sections, a summary of relevant work will be reported.

F. Chopard, Ch. Marvillet, J. Pantaloni [1994] tested three rectangular geometries: smooth, studded with in-line array, and studded with staggered array. In the tests, R-22 was evaporated in an upward flow for vertically configured plates. It was discovered that the experimental heat transfer coefficient was greatly influenced by heat flux. But, vapor quality and mass flow rate had little effect on heat transfer. It was also observed that the studded plates showed no significant enhancement.

T. Ohara, T. Yamamoto, H. Fujita [1991] performed R-12 evaporative studies for six plate finned channels that were oriented vertically. The test sections had identical cross sectional areas with ribs that were perpendicular to the flow. The rib height and spacing, or pitch, differed for each test section. The heat transfer coefficient results have determined that the tallest rib height and the smallest pitch provided the highest enhancement relative to the smooth channel. It was also observed that heat transfer coefficient increases with quality. Further, it was determined that the vapor Reynolds number must exceed a minimum in order to cause disturbances in the liquid before any enhancement can occur.

Robertson [1982, 1983] studied upward flow of nitrogen and R-11 in serrated-fin channels representative of the chemical process industry. Earlier experimental work was performed using Freon 11 (R-11) and nitrogen as working fluids. For the work performed with Freon 11, test conditions included mass fluxes up to 112 klb_m/ft^2-hr (150 kg/m^2-s), heat fluxes up to 1280 Btu/ft^2-hr (4 kW/m^2), and pressures from 44-102 psia (300-700 kPa). From the observed heat transfer coefficient trends, it was determined that nucleate boiling does not occur at such low heat fluxes leaving convective boiling as the main mode of heat transfer. It was also observed that heat transfer coefficients increase with mass flux (specifically, $G^{0.8}$) after the flow conditions have reached a critical Reynolds number. For the experiments performed with liquid nitrogen as the working fluid, results similar to the Freon 11 heat transfer trends were observed. Robertson claimed that there are two turbulent forced-convection boiling mechanisms present. The first mechanism occurs for qualities above 0.3 and mass fluxes of 60 klb_m/ft^2-hr (80 kg/m^2s) for liquid nitrogen in serrated fins. In this first mechanism, the heat transfer coefficient is a function of mass flux and quality. For the second mechanism, qualities below 0.3 and mass fluxes below 60 klb_m/ft^2-hr (80 kg/m^2s), heat transfer is a function of mass flux only. In this second mechanism, Robertson suggested that the onset of droplet entrainment may have an effect.

After the experimental work, Robertson [1984] proposed a two-phase flow model which takes into account local flow conditions and its effect upon liquid film boundary layers at the serrated fin. The model also considered droplet entrainment in the vapor core and its deposition of droplets from the vapor core to the fin. Once the film thickness has been determined, the film flow rate, film thickness, and film conductance was used to estimate the overall predicted temperature drop between the fin wall and the bulk fluid. By adjusting the parameter K, a non-dimensional deposition mass transfer coefficient, the model predicted the experimental data with good agreement.

T. N. Tran, M.W. Wambsganss, and D.M. France [1995] studied boiling heat transfer in small circular and rectangular channels. The emphasis of this work was to determine the mechanisms of heat transfer in small circular and non-circular channels which are representative of flow passages in compact heat exchangers. In this study, three fluids (R-12, R-113, R-134a) were tested over a mass flux range of 33-624 klb$_m$/ft^2-hr (44-832 kg/m^{2}s) and heat flux range of 1150-41280 Btu/ft^2-hr (3.6-129 kW/m^2) in horizontal test sections. The main result of the experiments was that heat transfer is completely dependent on heat flux and independent of mass flux and quality. This heat flux dependence implies that nucleate boiling dominates over convective boiling in small channels. The investigators attribute the dominance of nucleate boiling to the relatively small channel size. It seems that a channel size reduction reduces the critical wall superheat associated with the transition to nucleate boiling. Tran et al. reconciled the disagreement in conclusions relative to some investigators by considering how different experiments fall on different places on the boiling curve. The boiling curve is a plot of wall heat flux versus wall superheat which distinguishes between two distinct regions with a transition of nucleate and convective boiling. For this particular work, it was determined that this transition region occurs when the wall superheat is approximately 37.0 °F (2.75 °C). Tran et al. proposed a dimensional nucleate boiling dominant correlation in the form:

$$h_{tp} = C_3\, q''^{C_4} \tag{2.35}$$

where h_{tp} is in W/m^2-°C, q" is in kW/m^2 and C_3, C_4 are constants obtained by applying curve fits to the experimental data.

Carey and Madrusiak [1986] performed studies investigating film flow boiling in a vertical channel with offset strip fins. The objectives of the investigation were to obtain heat transfer measurements for vertical flow in channels with offset strip fins, gain insight between the two-phase flow behavior and heat transfer, and visually examine the effect of liquid Prandtl number on two-phase flow. In this investigation, water, methanol and n-butanol were tested over a mass flux range of 4.4-26.6 klb$_m$/ft^2-hr (5.8-35.5 kg/m^2-s) and a quality range of 0.05 to 0.7 in a vertical channel that was heated on one side. For the conditions tested, the flow was predominantly of the film flow type with the exception of the lowest qualities. From the results of the heat transfer measurements, it was determined that vertical film flow boiling heat transfer is a function of mass flux, quality and properties of the liquid with no heat flux dependence. Since convective boiling was the main mode of heat transfer for their experiments, a film flow model was proposed to try to model the experimental data. The model assumes that the liquid film is weakly turbulent, the liquid-vapor interface is smooth and there are no entrained droplets in the vapor core. Once the mass, momentum and energy relations have been manipulated to describe the two-phase flow, the correlation takes the form:

$$\left(\frac{h_{tp}}{h_l}\right)\frac{4.74\sqrt{A}\tan^{-1}[0.149\sqrt{\mathrm{Re}_l\,\mathrm{Pr}_l}]}{\mathrm{Re}_l^{n/2}\,\mathrm{Pr}_l^{1/6}}=\left[1+\frac{20}{X_{tt}}+\frac{1}{X_{tt}^2}\right]^{1/2} \qquad (2.36)$$

$$\mathrm{Re}_l=\frac{GD_h(1-x)}{\mu_l} \qquad (2.37)$$

Where h_{tp} is the two phase heat transfer coefficient, h_l is the single phase heat transfer coefficient for similar conditions, Re_l and Pr_l are the liquid Reynolds and Prandtl number, respectively, X_{tt} is the turbulent-turbulent Lockhart-Martinelli parameter and A, n are based upon single phase tests. The equation above has been simplified to describe channels that are heated on both sides.

In another study, Cohen and Carey [1989] investigated flow boiling in several vertical cross-ribbed channels. The various cross-ribbed channels differed by the angle relative to the flow and the distance between ribs. Experimental data was reported for R-113 and methanol for mass fluxes ranging from 30-173 $\mathrm{klb_m/ft^2}$-hr (40-230 $\mathrm{kg/m^2}$-s) and qualities ranging from 0.1 to 0.8. In this investigation, heat transfer coefficient measurements were taken in conjunction with visual observation as one side of the test section was replaced with a transparent polycarbonate cover. Since the flow regimes tested were predominately film flow, the investigators suspected that nucleate boiling would be completely suppressed, but it was observed that some nucleation in the corner regions just downstream of the ribs did occur. The presence of nucleate boiling was confirmed as heat transfer varied significantly with heat flux at low to moderate qualities. In the test section with the largest pitch angle relative to the flow, higher agitation of the two-phase flow suppressed nucleate boiling. This suppression was observed visually and by measurement as there was no dependence upon heat flux. This test section with the highest agitation also provided the highest enhancement. In general, geometries that provide high agitation suppress nucleate boiling and enhance overall heat transfer coefficients. The experimental results were compared to two correlation schemes, (1) a correlation developed by Carey and Madrusiak [1986], using $\Psi(X_{tt})$, in earlier work and (2) a round-tube correlation developed by Bennett and Chen [1980], using $F(X_{tt})$. When comparing experimental data to the correlations, there was good agreement for both the $\Psi(X_{tt})$ and $F(X_{tt})$ factors. This high coincidence of experimental and correlated results come from the highly enhanced test section, where nucleate boiling was suppressed. The experimental data of the other test sections with high nucleate boiling contributions was not resolved as the two correlation schemes only consider convective boiling.

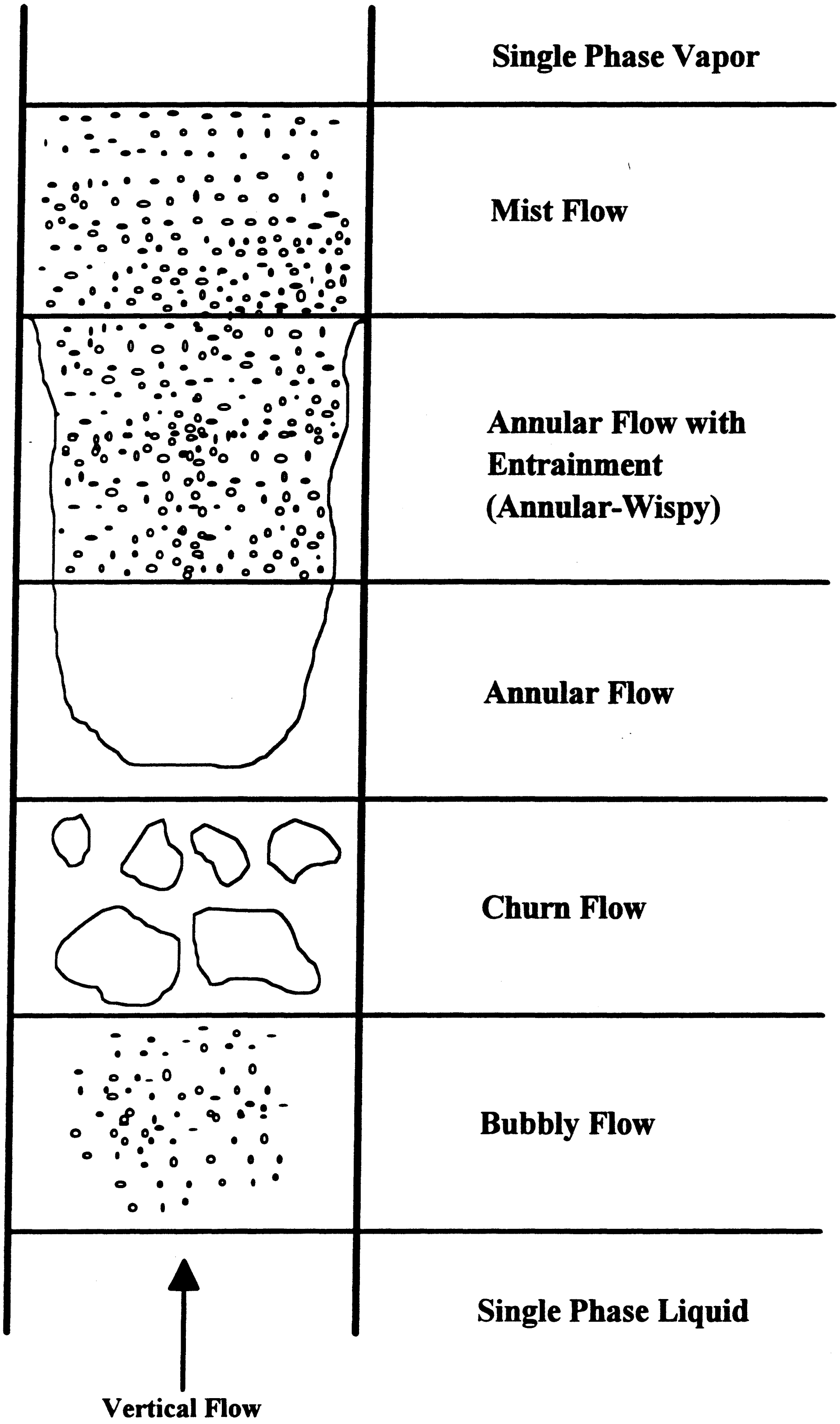

Figure 2.1 Visual Representation of Vertical Flow Regimes

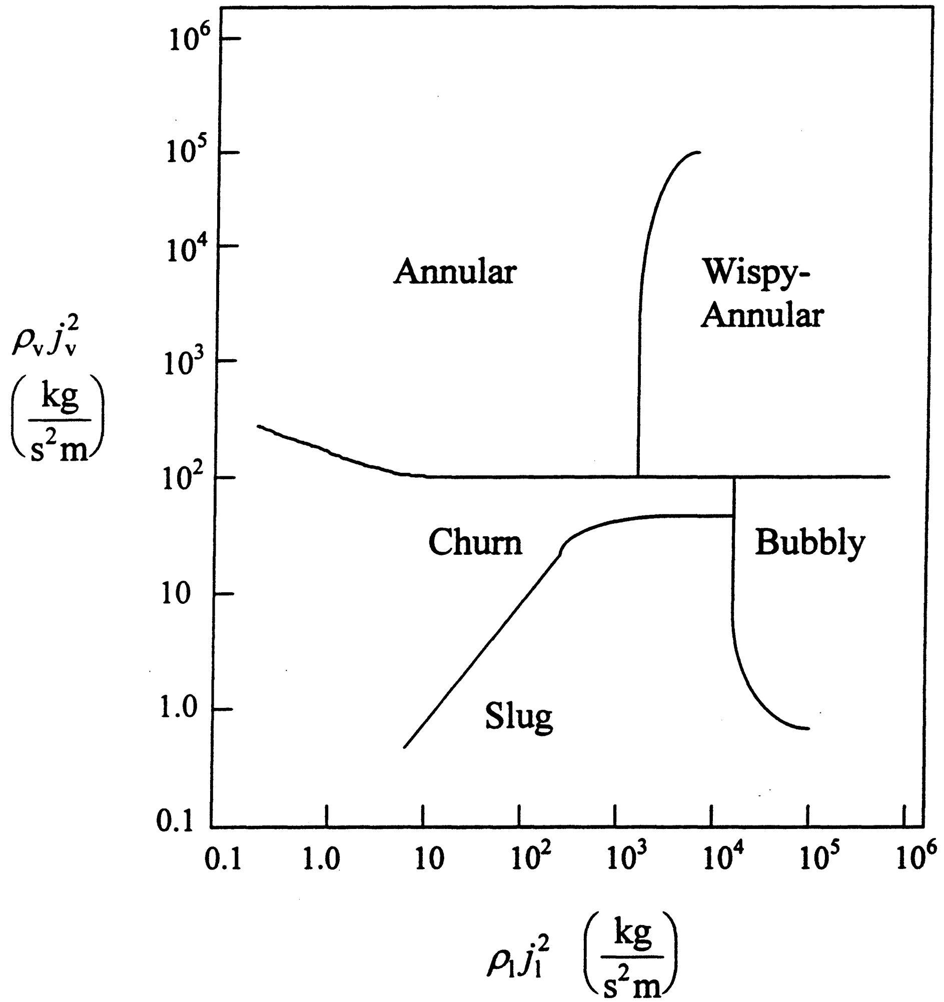

Figure 2.2 Vertical Flow Regime Map Proposed by Hewitt & Roberts [1969]

CHAPTER 3
Experimental Facility

In this chapter, a description of the facility utilized to perform this investigation will be presented. This facility which was located in the Mechanical Engineering Laboratory building at the University of Illinois at Urbana-Champaign was designed and built by Wattelet [1989] to study two-phase refrigerant-side evaporative flow regimes, heat transfer and pressure drop. Much of the details regarding this experimental apparatus have been described in detail by Panek [1991], Christoffersen [1993] and Wattelet [1994], therefore this chapter will only provide a brief summary of the facility.

3.1 Experimental Test Facility

The experimental facility incorporated four major systems: a refrigerant loop, a chiller loop, a plate test section, and a data acquisition system. In this section, a brief description of the hardware will be provided in the following subsections, while the data acquisition system will be described in the next section.

3.1.1 Refrigerant Loop

The purpose of the refrigerant loop was to provide precise control of the working fluid as it entered the test section. Conditions that were controlled during an experiment were mass flow rate, quality, heat input to the test section, and saturation temperature. Figure 3.1 shows a schematic of the refrigerant loop. First, subcooled liquid was drawn from the condenser by the variable speed gear pump. If the flow rate required at the test section was lower than the flow rate exiting the gear pump, a bypass line could be used to divert excess working fluid back to the condenser. Next, a Micro-Motion mass flow meter provided real-time measurement in order to adjust the flow rate as necessary. Following the flow meter, a preheater section provided heat to the working fluid in order to achieve the desired quality at the test section. In the test section, all temperature and pressure measurements were extracted and logged by the data acquisition. Finally, after the working fluid exited the test section, it was condensed by exchanging heat with the chiller system.

A variable-speed gear pump by Micropump was used to draw liquid from the condenser and provide the necessary flow to the refrigeration loop. With the use of varying the pump speed in conjunction with the bypass line, precise flow rates could be achieved. The motivation for the use of a variable-speed gear pump was to eliminate the need for a compressor and expansion device found in vapor-compression systems. Also, a gear pump provided the capability of testing pure working fluids without the influence of oil usually found in compressors.

After the gear pump, a mass flow meter manufactured by Micro-Motion was used to measure the flow rate. This Coriolis-type flow meter provided real time measurements by vibrating a U-tube to measure the flow. Another feature of this flow meter was that it had small orifices at the inlet and outlet to damp any small oscillations.

Once the refrigerant flow rate was measured, the refrigerant proceeded to the preheater section where the inlet quality to the test section was controlled. Structurally, the preheater was a three pass, horizontal, serpentine copper annulus with a 0.875 in. (22.2 mm) outside diameter and a 0.375 in. (9.53 mm) inside diameter. The smaller tube was secured by means of a spirally wrapped wire, concentrically situated inside the larger tube. This annulus configuration provided a smaller refrigerant charge requirement when compared to the 0.875 in. (22.2 mm) tube alone. Wrapped around the outer tube of the annulus were Kapton^{TM} strip heaters manufactured by Minco to provide the heat input. These heaters generated approximately 1700 Btu/hr (500 Watts) each and were controlled by four switches and a 115 Volt Variac. Two of the switches controlled approximately 5100 Btu/hr (1500 Watts) of power, one switch inputted 3400 Btu/hr (1000 Watts) and the remaining switch provided 1700 Btu/hr (500 Watts) to the preheater. The Variac provided precise control of the voltage to vary the heat input from zero to 3400 Btu/hr (1000 Watts). A combination of the switches and the Variac settings furnished the proper amount of heat to the refrigerant to obtain the desired quality entering the test section.

Once the refrigerant exited the preheater, it passed through the test section and condenser, which will be discussed in more detail in the subsequent sections.

3.1.2 Chiller System

In order to condense the two phase liquid exiting the test section, heat must be removed. This heat removal was accomplished by a counterflow, helical condenser that used a 50/50 solution of ethylene glycol and water as its coolant. This helical condenser configuration required a refrigerant charge between 6 and 13 lbm (3 and 6 kg), as compared to the approximately 20 lbm (9 kg) needed when using a shell and tube heat exchanger. With this helical condenser, charge control became an issue as this smaller heat exchanger could not act as a receiver. Therefore, frequent additions or deductions of refrigerant were required to maintain subcooled liquid conditions at the pump and preheater entrances.

The chiller system required a constant amount of ethylene glycol, approximately 50 lbm (23 kg). The ethylene glycol was held in a storage tank where a thermocouple monitored the temperature. Through a chiller control panel, a set point was established. Two antifreeze pumps cycled on and off in order to maintain the storage tank temperature within ± 2.0 °F (± 1.1 °C) of the set point. Another duty of the chiller controller was to control the amount of heat removal through an R-502 circuit. On the controller, a hi-low switch selected which of the two thermostatic expansion valves was active. One setting allowed large amounts of heat removal at high temperatures and the other setting provided additional cooling capacity at low temperatures. Once heat was extracted from the ethylene glycol loop, the R-502 system released heat to the municipal water supply at a maximum rate of 60,000 Btu/hr (17.5 kilowatts).

In order to maintain steady state conditions (i.e. constant saturation temperature) at the test section, the heat removal rate of the chiller system was matched to the heat input from the refrigerant loop condenser. This heat balance was accomplished by maintaining a constant heat removal capacity of the chiller system which would be matched with the heat input of the refrigerant loop condenser and false load heater. The following steps were used to establish a constant saturation temperature in the test section. First, an artificially low set point was inputted to the chiller control which would provide the constant heat removal capacity of the chiller system. Once the set point had been achieved, the chiller had a higher heat removal capacity than the heat rejected from the refrigerant loop. Next, the false load heater provided the additional heat to reach the desired saturation temperature. Finally, the false load heater could be adjusted to maintain the saturation temperature. Figure 3.2 is a schematic of the chiller system.

3.1.3 Test Section

The test section used for this study was modeled from existing aluminum plate-type evaporators found in current automobiles. The existing plates used in automotive evaporators could not be directly studied because of the difficulty of installation and instrumentation. This project was limited to the use of surface heaters (as opposed to water type heater arrangement) and thermocouples. Therefore, a test section was designed and built to accommodate the existing facility.

The test section consisted of two machined brass plates that were to be clamped together to simulate a single pass, plate-type heat exchanger. Several features were designed in order to accommodate control and instrumentation of this test section. The subsequent paragraphs will describe the various components of this test section.

Brass plates were chosen because of their relatively high thermal conductivity and favorable machinability characteristics. Since wall temperature measurements were to be utilized, a high thermal conductivity metal was chosen to provide a relatively constant material temperature between the external and internal surfaces. Due to the intricate design of the internal side, small machining tools were to be used which required a relatively soft material of favorable machinability characteristics (brass).

The internal design of the brass plates simulated a commonly used flow scheme for plate-type heat exchangers. Another design constraint was to accommodate the existing experimental facility. Figure 3.3 shows a schematic of the machined surface of the plates. First, the fluid entered the test section via a ½ inch O.D. tube which was brazed to the top brass plate. From the tube, the fluid experienced a 90-degree deflection into the test section where the machined channel was approximately the size of the tube and expanded to the full cross section of the flow passage, 3.051 inch x 0.118 inch (77.5 mm x 3.0 mm). This expansion existed in order to reduce the chance of any "dead spots" or recirculation of the flow before entering the next part of the test section. Next, the fluid would pass through a flow straightening section to provide uniform flow to the main part of the test section. Once the flow of fluid stabilized in the flow straightening section, it entered the main part of the test section where there were circular protrusions on the wall which caused turbulence. All the temperature and pressure measurements were taken in this section. Finally, the fluid entered a contraction so that it could exit a ½ inch (12.7 mm) O.D. tube which was also brazed to the top plate.

Since the circular protrusions increase the wall area as well as cause turbulence, the possibility of enhancement of heat transfer exists. When aluminum plates are formed in production, dimples are stamped onto the heat transfer surface. These dimples should provide heat transfer enhancement as well as structural strength. As two aluminum plates were brazed together, mating the tips of these dimples also provided structural support for the flow passage. For this test section, the dimples were formed by using a 45-degree end mill which cut in a circular pattern. The resulting obstruction was a frustum, truncated cone, that had a 0.197 inch (5.0 mm) lower base, 0.0787 inch (2.0 mm) upper base and height of 0.0591 inch (1.5 mm). The centerline to centerline distance between rows of dimples was 0.256 inch (6.5mm). This geometry did not completely replicate the production dimples, but provided a close approximation.

Temperature measurements were made by the use of wall mounted and probe thermocouples. The wall mounted thermocouples were located at various positions throughout the brass plate. To accommodate the wall thermocouples, sixteen holes were drilled near the centerline, approximately 1.693 to 1.890 inch (43 to 48 mm) deep and 0.0394 inch (1.0 mm) below the machined surface, at specific locations. In order to provide good contact between the end of the drilled hole and thermocouple, the thermocouple junction was welded together to produce a ball like bead. When the thermocouple bead was placed into the drilled hole, a high conductivity silicon paste was used to cover the bead to ensure that no air pockets surrounded the thermocouple end. In order to measure bulk fluid temperatures, a type-T thermocouple probe with stainless steel sheathing was inserted into the fluid flow before and after the test section of the brass plate. To accommodate the thermocouple, a hole was drilled and tapped to allow proper mounting of a compression fitting that could secure the probe. Several diagnostic test runs were performed to assure acceptable temperature measurements.

Along with temperature measurements, pressure measurements were taken during each test run. Next to the compression fittings for the probe thermocouples, holes were drilled and an eighth inch O.D. copper tube was brazed into it which served as a pressure tap. The pressure tap at the inlet of the test section was connected to an absolute pressure transducer and is the high side of a differential pressure transducer. The low side of the differential transducer was attached to the outlet pressure tap. These pressure measurements provided a check on the inlet and outlet saturation temperatures as well as pressure drop data.

To provide the appropriate heat flux to the test section, surface heaters were mounted to the appropriate part of the test section. These 3 x 10 inch (76.2 x 254 mm) surface heaters were manufactured by Minco which feature an aluminum foil backing to ensure uniform heating. During installation, a high conductivity silicon paste was applied between the aluminum foil back of the surface heater and the outside part of the test section. These heaters were positioned opposite side of the main or "dimpled" part of test section. In order to reduce the chance of heat conduction away from the section of interest, two sets of 0.0394 inch (1.0 mm) grooves were milled on the inlet and outlet edges of the "dimpled" part of the test section. Once the heaters were installed to the upper and lower plates, they were wired in parallel to a 115 Volt Variac which controlled the heat settings.

Once the instrumentation had been installed, the two brass plates were to be mated with an O-ring strip around the periphery to provide a single channel arrangement that did not leak. The union of the upper and lower brass plates was accomplished by clamping them between two ½ inch (12.7 mm) thick Lexan polymer pieces and several steel Uni-Strut (standard C-configuration) pieces. The Lexan (polycarbonate) was chosen because of its low thermal conductivity (insulating properties), desirable mechanical properties, and availability. These Lexan pieces were machined to accommodate the brass plates, plumbing and instrumentation. Clamping force was achieved by using eight pairs of steel Uni-Strut pieces that bolted the Lexan and brass pieces together. Before the brass plates could be joined, locator pins were installed to ensure proper alignment of the internally machined surfaces. Also, a groove was milled along the outer perimeter of the machined surface that accommodates a 3/32 inch (2.38 mm) O-ring gasket to ensure that the working fluid does not escape during testing. Figure 3.7 shows the different pieces that were clamped together.

3.2 Data Acquisition System

The data acquisition system was used to monitor and control the experimental apparatus during operation and record all pertinent measurements when test conditions have been met. The data acquisition system consists of the following components: a Macintosh II computer, four Strawberry Tree^{TM} data acquisition boards, six Strawberry Tree^{TM} terminal panels, and a data acquisition program called Analog Connection Workbench^{TM}.

The interfaces between the thermocouple outputs and the Strawberry Tree^{TM} data acquisition boards were four T-21 terminal panels with aluminum, isothermal plates. Other sensors, such as pressure, power, and flow rate transducers, provided signals to the data acquisition boards through T-51 terminal panels. Finally, the false load output signal was relayed to the main logic controller by a T-51 terminal panel.

Terminal panels were linked to the data acquisition boards via a 50 pin ribbon connector. The data acquisition boards consisted of two 8 channel boards with analog output capability, model numbers ACM2-16-8A and ACM2-12-8A. In the model numbers, 16 and 12 denote bit precision. In addition, there were two 16 channel data acquisition boards: ACM2-16-16. In total, the system had the capability of accepting 48 analog inputs and providing 4 analog outputs. Typically, data was sampled at 1 Hz for the data acquisition configuration that was chosen.

Along with the hardware, Strawberry Tree^{TM} provided software to run the data acquisition system. This icon driven program displayed and recorded signals from the data acquisition hardware. In the program, computation was done using calculation blocks which stored the necessary calibration curves. In terms of control, the false load heater was manually controlled through the continual adjustment of one of the calculation blocks. Once flow conditions satisfied test requirements, the data was logged to disk in a tab-delimited file.

3.3 Instrumentation

This section will describe the various measurement devices used in the experimental apparatus. These devices include flow meters, power transducers, thermocouples, and pressure transducers.

3.3.1 Mass Flow Measurements

A Coriolis-type mass flow meter manufactured by Micro-Motion was used to measure the mass flow rate of the working fluid circulating through the refrigerant loop. This flow meter, model D-12, featured two small orifices located at the inlet and outlet which help dampen any oscillations in the flow.

Another flow meter was placed in the chiller system which measures the flow rate of the ethylene glycol. The output of the Flow Technology turbine flow meter was necessary for logic controller to maintain the set point temperature. Since the viscosity of the ethylene glycol mixtures vary considerably with temperature, the flow meter was calibrated at three different viscosities to account for this effect.

3.3.2 Power Measurements

Three Ohio Semitronics Watt transducers were used in the experimental facility. The first transducer, model PC5-49D92, measured the heat rate at the test section. The next transducer, model PC5-50D292, measured the power controlled by the four preheater switches. The last transducer, model PC5-010D, monitored the power input provided by the Variac controller. All three devices were tested at the factory at an uncertainty of 0.2% of the full scale reading.

3.3.3 Pressure Measurements

Four pressure transducers were installed on the refrigerant loop to monitor system performance and provide a secondary check on the saturation temperature. An absolute

BEC strain-gage type pressure transducer took measurements at the inlet to the preheater. The output of this preheater pressure transducer, range of 0-300 psia (0-2100 kPa), was used to determine the amount of subcooling in the liquid. Another pressure transducer, same as the preheater transducer, was used to measure the pressure at the inlet to the test section. For two phase flow, this inlet pressure measurement was used to confirm the bulk fluid temperature measurement, as saturation temperature could be calculated. For single phase flow, this inlet pressure measurement determined the amount of subcooling available at the test section entrance. The last absolute pressure transducer, manufactured by Sentra with a range of 0-1000 psia (0-6900 kPa), measured the pressure at the inlet of the gear pump. These pressure measurements are used to determine the amount of subcooling at the pump entrance. If there is insufficient subcooling, the pump does not operate at maximum efficiency. Finally, in order to determine the pressure drop across the test section, a Sensotec differential pressure transducer with a range of 0-5 psi (0-35 kPa) was used. All four devices were calibrated using a dead weight tester with an uncertainty of 0.3% of the full scale reading.

3.3.4 Temperature Measurements

Thermocouples used in the experimental facility were calibrated using a Neslab constant temperature bath and NIST traceable, high precision thermometers. During calibration, an ice bath was utilized as reference state and voltage differences were used in the calibration procedures. This ice bath reference was adopted in favor of the cold junction sensor feature of the data acquisition system. From previous work, it was found that the cold junction feature had large variability in temperature measurements relative to the position on the terminal panel. The thermocouples along with the different terminal panels were calibrated over a range of 18 to 104 ^{o}F (-8 to 40 ^{o}C). Uncertainty of the temperature measurements was estimated to be $\pm 0.36\,^{o}$F ($\pm 0.2\,^{o}$C).

Temperature measurements were utilized to determine surface and bulk fluid temperatures. For the surface temperatures, holes were drilled into the test section to accommodate the prepared thermocouples, as described in section 3.1. To determine bulk fluid temperatures, thermocouples protected by a stainless steel sheath were extended into the refrigerant flow. These probes were held in place with compression fittings and were located at the following locations: the inlet of the pump, before the preheater, and the entrance to the test section. At the inlet to the pump and preheater, the temperature measurement was used to determine the amount of subcooling and the refrigerant's enthalpy. At the test section entrance, the temperature measurement was compared to the pressure measurement as a check on saturation temperature.

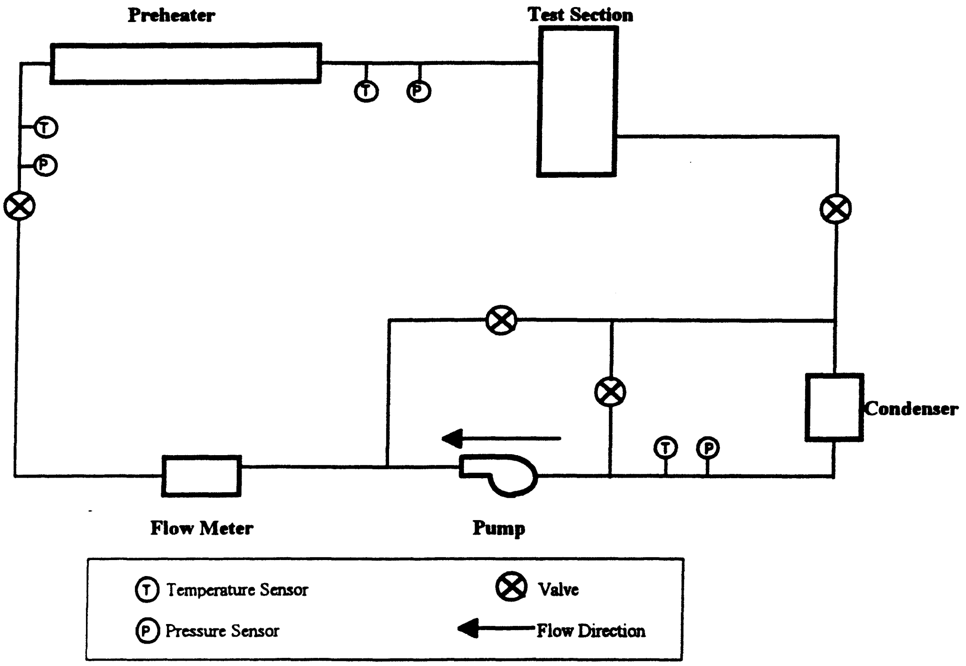

Figure 3.1 Schematic of Refrigerant Loop

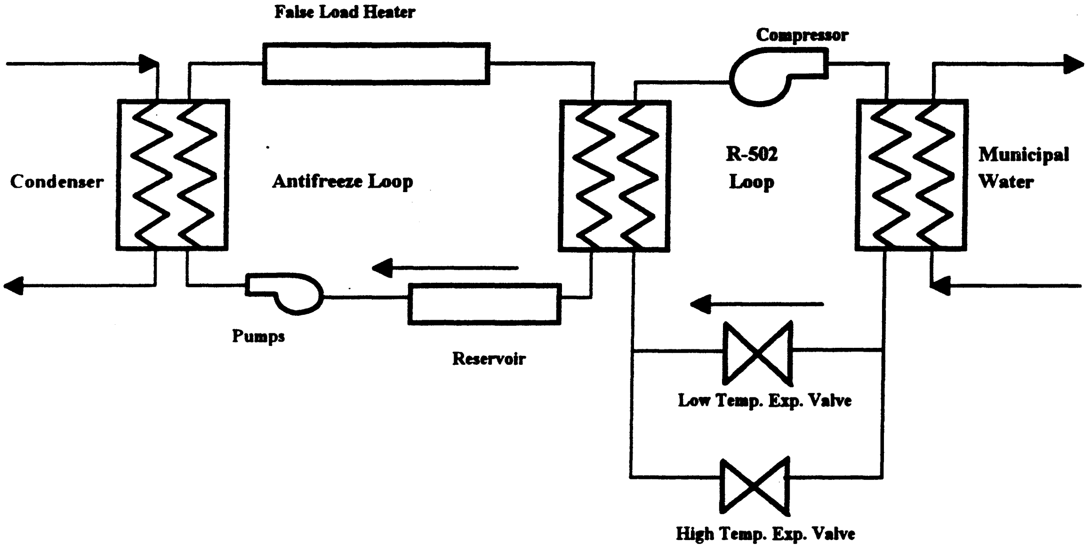

Figure 3.1 Schematic of Chiller System

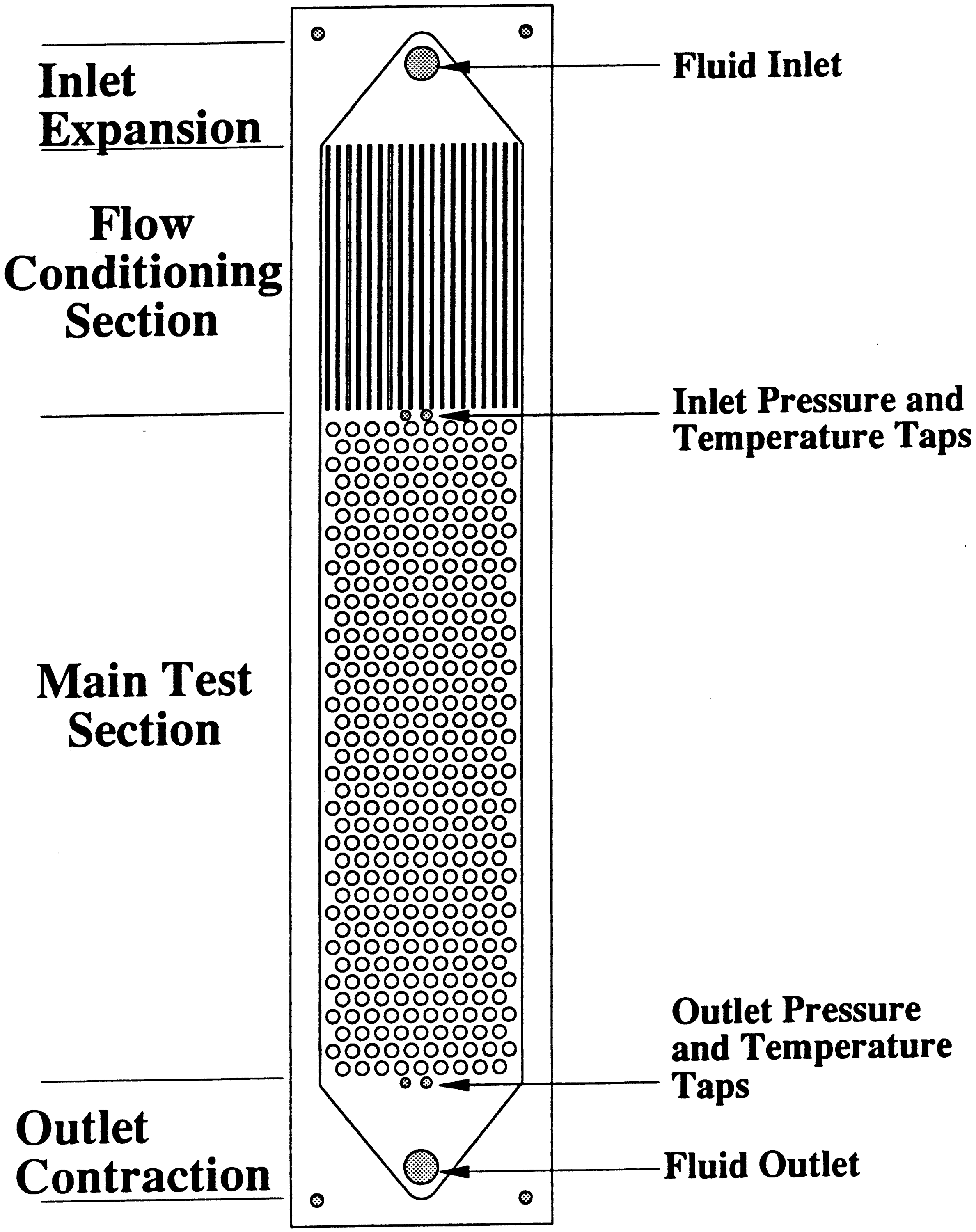

Figure 3.3 Schematic of Test Section

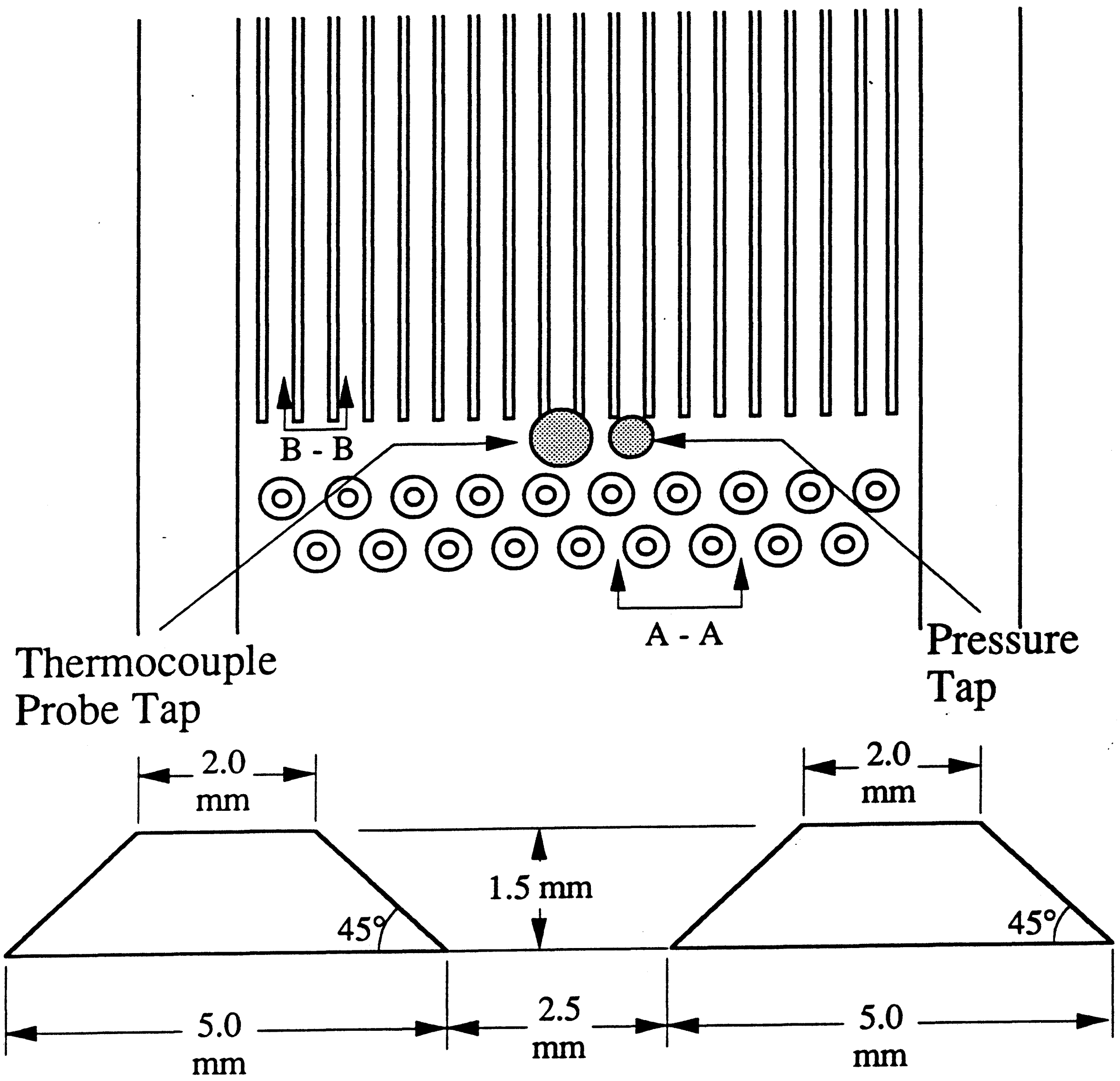

View A - A

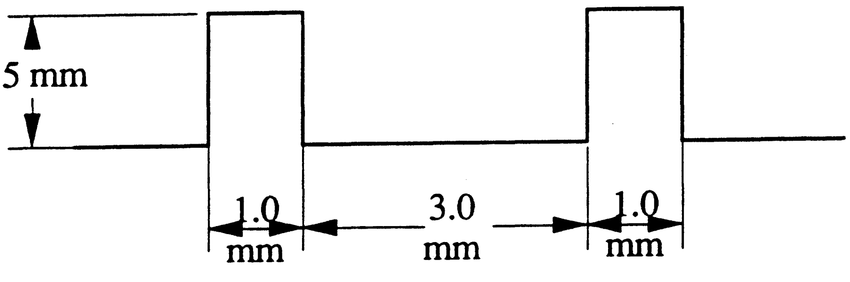

View B - B

Figure 3.4 Schematic of Flow Obstructions

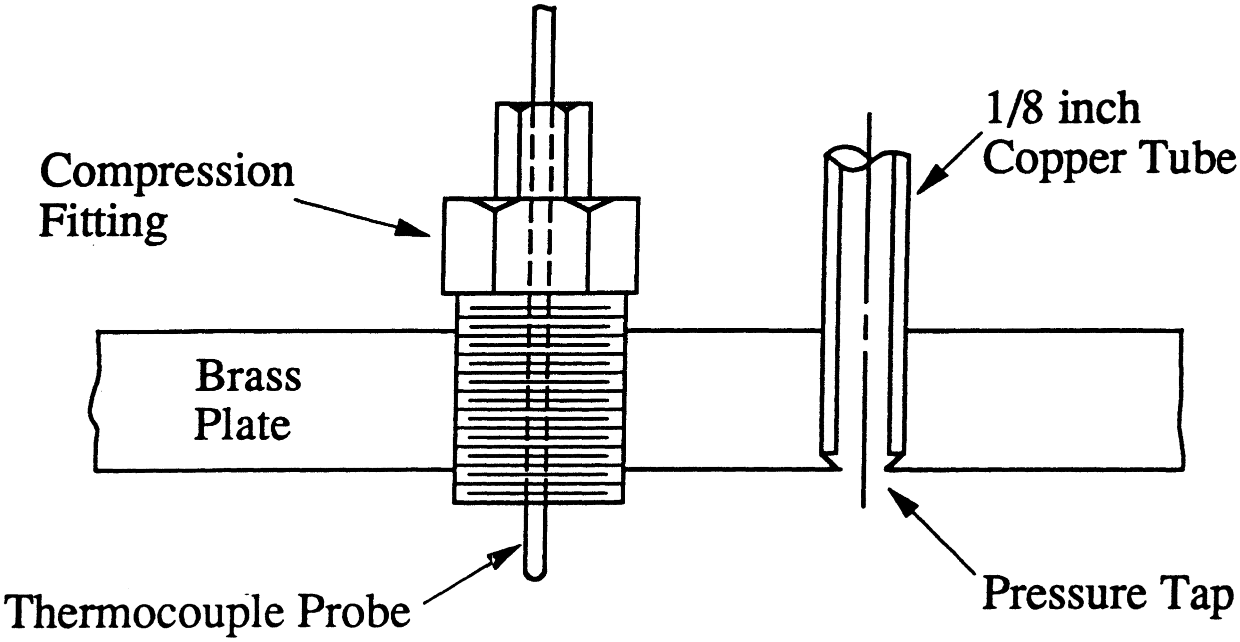

Figure 3.5 Schematic of Thermocouple and Pressure Tap Mountings

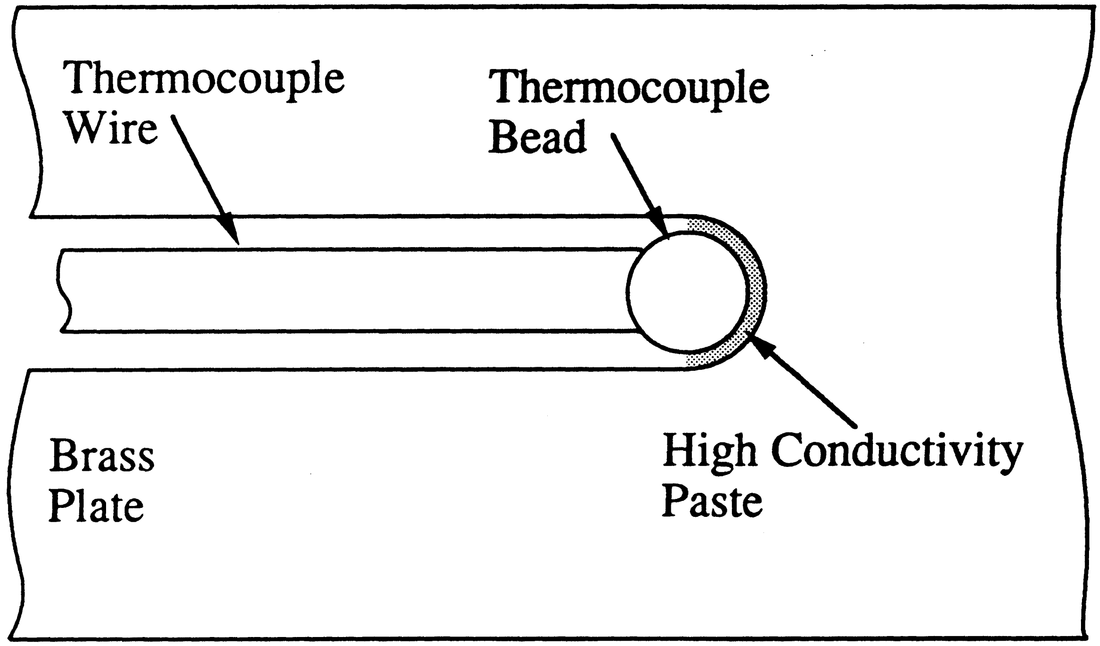

Figure 3.6 Schematic of Wall Thermocouple Mounting

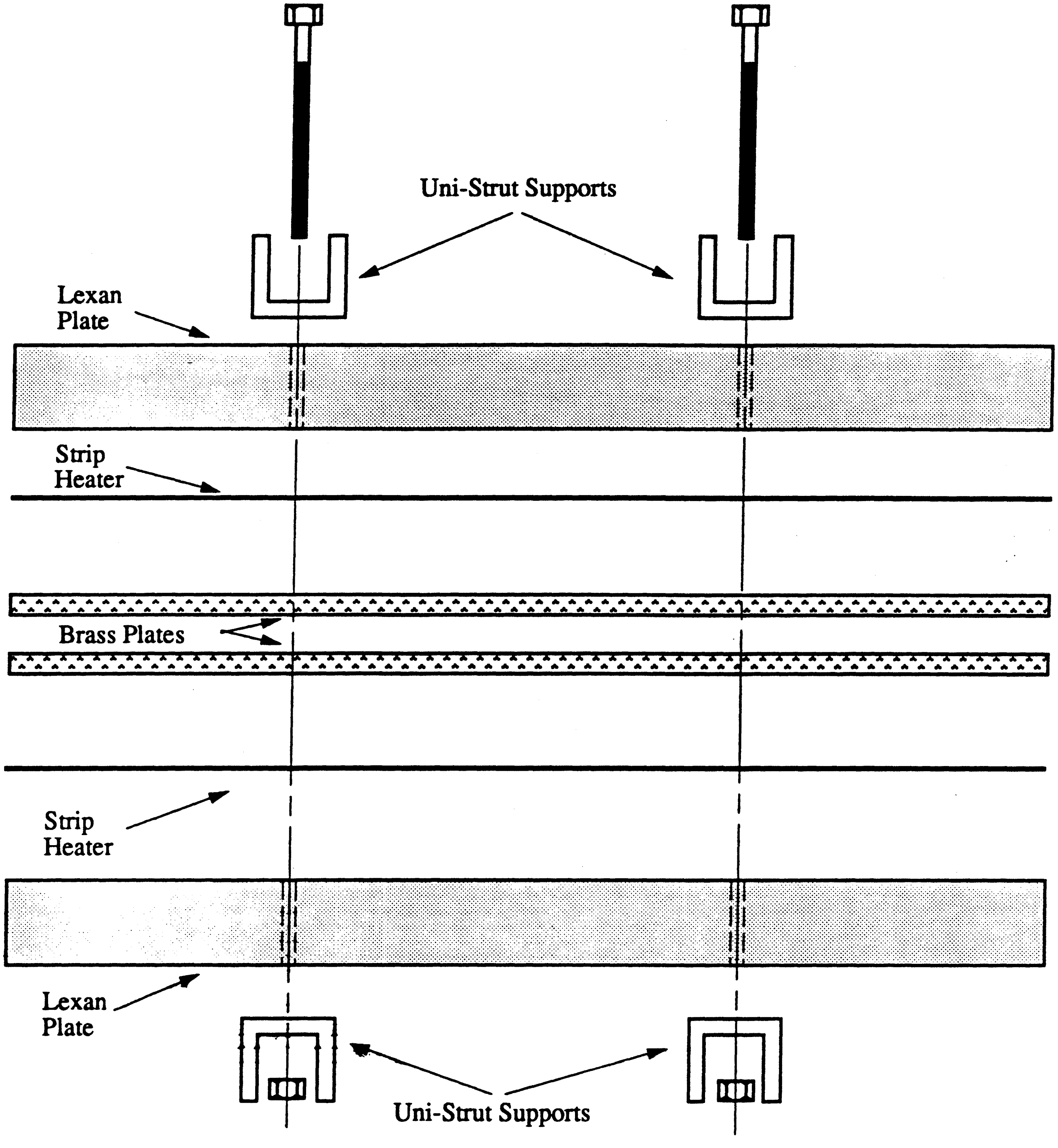

Figure 3.7 Schematic of Clamping Configuration

CHAPTER 4
Experimental Procedure

In order to provide experimentally consistent results, a series of steps were followed to ensure the validity of data collection. This chapter will outline the preparation of the experimental facility and the procedures necessary to obtain the data. Also, calculations of heat transfer coefficients, system heat gains, and experimental uncertainties will be discussed. Additionally, testing to validate proper operation of the experimental facility will be presented. Finally, the range of conditions for the collected data will also be reviewed.

4.1 Experimental Facility Operation

This section comprise two parts. First, the preparation procedures necessary to run a new set of tests will be described. These steps are performed only once prior to the testing of a new refrigerant or test section. The next section will present the regular operation of the experimental apparatus.

4.1.1 System Preparation

Prior to testing a new refrigerant or test section, the refrigerant loop was evacuated to remove any contaminants that may be present. Once the refrigerant loop was evacuated, the system was divided into an upper and lower section by two ball valves. By monitoring any pressure gains, system leaks could be determined. Since the loop was sectioned, the location of the leak(s) could be found more readily.

This vacuum method could only determine if a leak existed, but it could not really identify the exact location. To determine the exact location of the leak, the system was pressurized with refrigerant (R134a) to approximately 72 psia (500 kPa). After the system was charged with a high pressure vapor, the loop was divided into an upper and a lower section. Rapidly decreasing pressure in either sections indicated the presence of a leak. To determine the exact location of a leak, an electronic halogen leak detector and/or a soapy water solution was used to check all connections and fittings. Once the leak was found, tightening, re-soldering, or replacing any components was done. After the repairs, the refrigerant loop was pressurized and monitored overnight. If the pressure remained constant, the system was assumed to be leak free and ready for testing.

4.1.2 Operating Procedure

Before taking any heat transfer measurements, initial system testing was performed to ensure all the components of the experimental facility were in proper working order. First, the power and water to the facility was activated. Next, the ice bath was replenished with a fresh mixture of crushed ice and water. Once the data acquisition computer was operational, temperature and pressure measurements were inspected to determine any potential problems. Then, the variable speed gear pump was turned on to establish refrigerant flow. Next, the chiller pumps and compressor were started and a set point temperature to the ethylene glycol was established. The next step was to supply power to the preheater and test section heaters. Finally, the apparatus was fully operational and test conditions could be set accordingly.

The controlled test parameters included: mass flux, heat flux, inlet quality, and saturation temperature. First, mass flux was controlled by adjusting the variable speed gear pump and bypass line. Next, the inlet quality to the test section was controlled by inputting the proper amount of heat to the preheater. Continual adjustment of the preheater and mass flow was necessary, since they were contingent upon each other. After the mass flux and inlet quality stabilized, the test section heat flux was set. Finally, the saturation temperature at the test section entrance was adjusted by matching the heat rejection of the refrigerant loop and false load heater with the cooling capacity of the chiller system.

Once the controls to the experimental apparatus were established, the refrigerant loop was allowed to reach steady state at the prescribed saturation temperature. Steady state was achieved when the following parameters met the range of target values: mass flux, ±5%, heat flux, ±5%, and saturation temperature, $\pm 0.36\,^{\circ}F$ ($\pm 0.2\,^{\circ}C$). At this time, the data was logged for one minute. This data was then exported to a data reduction program where calculation could be performed.

4.2 Data Reduction

The data logged from the experiment was extracted into a Microsoft Excel spreadsheet where all pertinent calculations were performed. In the spreadsheet, test section dimensions and thermophysical property curve fits of the working fluid (R134a) were referenced extensively by the calculations. Curve fits, Appendix A, for the refrigerant were generated by the data provided by Dupont. For each test run, all the raw data was averaged to calculate the experimental heat transfer coefficient. Finally, the results were transferred to a clear and concise ledger sheet that was saved for hard copy.

Heat transfer coefficients, both single-phase and two-phase, were calculated from Newton's law of cooling, which is as follows:

$$h = \frac{q / A_s}{\left(\overline{T}_s - \overline{T}_b\right)} \tag{4.1}$$

In this equation, A_S represents the internal heat transfer surface area, q is the heat input to the test section, $\overline{T}_s$ is the average surface temperature at a particular location, and $\overline{T}_b$ is the interpolated value of bulk fluid temperature. Since the surface temperatures were measured approximately 1.0 mm away from the surface to liquid interface, conduction effects were taken into account and corrections were made. Also, axial heat conduction away from the main part of the test section was minimized by reducing the cross sectional area, but it was still incorporated into the data reduction. Minimal axial heat conduction has been verified by experimental energy balance tests.

Heat discrepancies were determined during single-phase energy balance testing. Discrepancies were determined by comparing the heat input to the heat absorbed by the liquid for a particular location (preheater and test section). Since the test section had a large amount of material (brass) and only a particular portion of the test section was of interest, there was some heat loss due to axial conduction effects. Test section heat losses for single phase were within 10%. For two-phase tests, where the surface to liquid interface heat transfer coefficient will be several times higher, this would provide a lower resistance for the flow of heat into the fluid and reduce axial conduction effects. In order to account for this heat loss, a correction factor was included in the data reduction program. Other energy balance tests were performed for the preheater and a heat gain was found to be on the order of 34 Btu/hr (10 Watts).

In order to determine the inlet quality to the test section, an energy balance was calculated for the preheater section of the experimental apparatus. When the working fluid entered the preheater, it was in a subcooled state. This subcooled liquid was assumed to have an enthalpy that is approximately equal to the enthalpy of the saturated liquid at the same temperature. As discussed by Wattelet [1994], this approximation resulted in a negligible error. The enthalpy of the refrigerant was defined in the following equations:

$$i_{preheater,exit} = \frac{q_{preheater}}{\dot{m}} + i_{preheater,\ inlet} \tag{4.2}$$

where

$$i_{preheater,\ inlet} = i_l\left(T_{preheater,\ inlet}\right) \tag{4.3}$$

In the preceding equations, i is the enthalpy of the refrigerant at a particular location, i_l is the saturated liquid enthalpy which is a function of fluid temperature, and $\dot{m}$ is the mass flow rate of the refrigerant. Since the outlet of the preheater is essentially the inlet to the test section, the enthalpy of the refrigerant exiting the preheater is equal to the enthalpy entering the test section.

$$i_{test\ section\ inlet} = i_{preheater,\ exit} \tag{4.4}$$

Therefore, the inlet quality to the test section is:

$$x_{test\ section,\ inlet} = \frac{i_{test\ section,\ inlet} - i_l\left(T_{test\ section,\ inlet}\right)}{i_{lv}\left(T_{test\ section,\ inlet}\right)} \tag{4.5}$$

Also, the change in quality of the test section due to the input heat is:

$$\Delta x = \frac{q_{test\ section}}{\dot{m} \cdot i_{lv}\left(T_{test\ section,\ avg}\right)} \tag{4.6}$$

For this particular test section, there was very little fluid temperature change since the pressure drop was very low for most cases.

4.3 Single Phase Testing

Single phase testing was performed to determine energy balances over the test section. This preliminary testing was necessary to determine if the heat input could be accounted for by the heat absorbed by the fluid in the main part of the test section. There was some concern regarding heat loss since axial conduction could possibly transfer heat away from the main part of the test section. Taking this effect into consideration, at the boundaries of the test section, two parallel 0.04 inch wide by 0.015 inch deep (1.0 mm x 3.85 mm) grooves were milled to reduce the area for conduction. From experimental single phase test runs, the controlled heat input and the change in enthalpy of the fluid was within 10%. It was assumed that for two-phase tests, where the surface to fluid heat transfer coefficient were several times higher, the relative conduction effects were much smaller.

Once the energy balance of the test section was acceptable, single phase tests were performed.

4.4 Uncertainty Analysis

Experimental uncertainty was calculated by a sequential perturbation method described by Moffat [1988]. In this calculation, a base heat transfer coefficient was determined from experimental data. Next, each independent variable used to calculate the heat transfer coefficient was perturbed by its uncertainty. From each perturbation, a new heat transfer coefficient was calculated and the square root of the sums was taken. The difference between this perturbed value and the base values is the maximum error. The following equation summarizes this method.

$$\partial h=\left[\left(\frac{\partial h}{\partial \dot{Q}_{TS}}\partial \dot{Q}_{TS}\right)^2+\left(\frac{\partial h}{\partial d_i}\partial d_i\right)^2+\left(\frac{\partial h}{\partial L_{HX}}\partial L_{HX}\right)^2+\left(\frac{\partial h}{\partial \overline{T}_s}\partial \overline{T}_s\right)^2+\left(\frac{\partial h}{\partial \overline{T}_b}\partial \overline{T}_b\right)^2\right]^{1/2} \tag{4.7}$$

Table 4.1 Parameter Uncertainty

Parameters	**Uncertainties**
Inside hydraulic diameter, d_h	± 0.003 in. (0.08 mm)
Heated length, L_{HX}	± 0.25 in. (6.35 mm)
Surface temperature, $\overline{T}_s$	0.36 °F (0.2 °C)
Bulk fluid temperature, $\overline{T}_b$	0.36 °F (0.2 °C)
Test section heat input, $\dot{Q}_{TS}$	±10%

From the parameter uncertainties, experimental uncertainties in the heat transfer coefficients were typically 15%. Higher uncertainties occurred for conditions when the surface to fluid temperature difference was relatively low. The uncertainties in heat transfer coefficient are present with the experimental data in Appendix A.

4.5 Test Matrix

The conditions in which the experiments were conducted are shown in Table 4.2. Test parameters were chosen to simulate typical conditions found in a plate-type evaporator for a single pass. For the higher mass fluxes tested, inlet saturation temperature were higher than desired, due to facility limitations. In order to achieve a certain quality at the higher mass fluxes, large heat inputs to the fluid were required which was beyond the heat rejection capability of the system condenser.

Table 4.2 Test Conditions

Parameter	**Conditions**
Inlet saturation temperature	41-68 ^{o}F (5-20 ^{o}C)
Mass flux	37-220 klb$_m$/ft^2-h (50-300 kg/m^2-s)
Inlet quality	0.2-0.8
Test section heat flux	1600-8000 Btu/ft^2-h (5-25 kW/m^2)

CHAPTER 5
Experimental Results

In this chapter, the heat transfer experimental results will be presented and discussed. The effects of the range of parameters and the orientation of the flow will be analyzed. Once the various effects have been analyzed, several aspects of the test conditions and the physical properties of the fluid will be explored in order to better understand the heat transfer mechanism.

5.1 Heat Transfer Results

The heat transfer results presented in this chapter will be in the form of Nusselt number, Nu. The use of this dimensionless number will avoid confusion due to any preference for a unit scheme (i.e. SI or English). In order to provide consistency with the mass flux calculation, the Nusselt number is based upon the hydraulic diameter of the minimum cross sectional area of the flow channel, as shown in the following equations.

$$Nu=\frac{h_{tp}D_h}{k_l} \tag{5.1}$$

based upon,

$$D_h=\frac{4A_{\min}}{P} \tag{5.2}$$

5.2 Mass Flux, Heat Flux and Quality Effects

In this section, the heat transfer effects due to the controlled test parameters will be presented. In the analysis of this data, it must be noted that these effects are interrelated and any conclusions should be based upon all the parameters.

For upward flow, figures 5.1 through 5.5 show the experimental Nusselt number variations with quality and heat flux for the various mass fluxes. This quality and heat flux dependence verifies that both nucleate and convective boiling mechanisms are present. For the lowest heat flux tests, 960 - 1600 Btu/ft^2-h (3 - 5 kW/m^2), the Nusselt number increases with quality for the various mass fluxes which is indicative of convective boiling. As heat flux increases, there is some heat transfer enhancement depending upon quality and mass flux. Particularly at the lower qualities for each mass flux some heat flux dependence is observed. For all mass flux tests, any heat flux dependence vanishes as quality increases. Also, the dependence upon heat flux increases with mass flux. This heat flux and mass flux relation is counter intuitive and will be addressed in subsequent sections.

Once the upward flow testing was completed, the test section was repositioned 180° for downward flow testing. Regarding heat transfer observations, most of the mass flux, heat flux and quality trends mimic the upward flow results, as shown in figures 5.6 through 5.9. The main departure from the upward flow heat transfer trends is that the heat flux dependence for the downward flow configuration remains consistent throughout the mass flux range. Even at the lower mass fluxes, G = 37 & 56 klb_m/ft^2-hr (50 & 75 kg/m^2-s), downward flow exhibits some heat flux dependence at the lower qualities. The next section will compare and discuss the discrepancy between the upward and downward flow configuration.

5.3 Upward and Downward Flow Comparison

In figures 5.10 through 5.13, heat transfer coefficients are directly compared for the same mass flux, heat flux and quality. From figure 5.10, it is evident that at the highest tested mass flux, G = 110 klb_m/ft^2-hr (150 kg/m^2-s), upward and downward flow produce nearly the same results. As mass flux decreases, figures 5.11 through 5.13 suggest that the upward flow configuration provides higher heat transfer coefficients when compared to the downward flow conditions. This heat transfer enhancement due to upward flow is particularly apparent at the higher qualities. In figure 5.13, at a mass flux of G = 37 klb_m/ft^2-hr (50 kg/m^2-s), the downward flow heat transfer results show a greater heat flux dependence relative to the upward flow heat transfer results. Essentially, upward flow at the lower mass fluxes suppresses nucleate boiling while enhancing convective boiling characteristics as evidenced by the increased heat transfer performance.

These differences in nucleate and convective boiling contributions and heat transfer performance is a result of two phase flow variations at the same mass flux due to the upward or downward configuration. Due to the vertical nature of the flow, it is assumed that the film flow regime would dominate for the range of mass fluxes tested. Slight variations in the film flow regimes could possibly account for the heat transfer differences such as the vapor-liquid velocities and possible dead spots behind the dimples relative to the flow. Since flow visualization was not possible with the experimental apparatus, variations in the upward or downward flow configurations could not be observed.

5.4 Heat Transfer Mechanism

In the literature, there have been some inconsistencies regarding the heat transfer mechanisms in two-phase evaporative heat transfer in small channel, variable geometries. One method used by Steiner and Taborek [1992] to determine if one or both heat transfer mechanisms are present is to plot heat flux versus $\Delta T_s = (T_w - T_{sat})$. When ΔT_s is below the onset of nucleate boiling, the dominant heat transfer mechanism is convective boiling which is represented by a slope of unity on this heat flux versus ΔT_s plot. Also, on this heat flux versus ΔT_s plot for convective boiling, different mass flows will be represented by parallel lines with a slope of unity. At the onset of nucleate boiling, these parallel lines begin to curve towards each other. Once these lines converge to a single line, nucleate boiling is the dominant mode of heat transfer. In figure 5.14, a schematic of typical boiling curves are shown.

In figures 5.15 and 5.16, plots of heat flux versus ΔT_s for upward and downward flow are presented. Both configurations show a transition between the convective and nucleate boiling region. Upon further inspection, the upward flow plot illustrates that the lines have slopes closer to unity relative to the downward flow configuration. This observation indicates that the upward flow configuration has heat transfer characteristic that is represented by the earlier part of the transition region, as shown in figure 5.14. In the earlier portion of the transition region, nucleate boiling begins to contribute, but convective boiling is still the main mode of heat transfer. In the later portion of the transition region, nucleate boiling plays a larger role in the mechanism of heat transfer, as illustrated by downward flow in figure 5.16. Therefore, for these experiments, upward and downward flow at low mass fluxes represent different portions of the transition region for traditional boiling curves.

5.5 Data Comparison

The data has been compiled into a comprehensive format for each flow configuration. For the first compilation, the experimental data is transformed into dimensionless parameters. These dimensionless parameters take several thermophysical properties into account. In figures 5.17 and 5.18, two plots that represent the upward and downward flow configurations are described with the following parameters:

$$X_{tt} = \left(\frac{\rho_v}{\rho_l}\right)^{0.5} \left(\frac{\mu_l}{\mu_v}\right)^{0.15} \left(\frac{1-x}{x}\right)^{0.35} \tag{5.3}$$

$$\frac{Nu}{\mathrm{Re}_l^{0.7}\,\mathrm{Pr}_l^{0.3}} \tag{5.4}$$

The Lockhart-Martinelli parameter, X_{tt}, indicates the relative effects of turbulent flows for the liquid and vapor phases which take quality, density ratio and viscosity ratio into account. Also, the Nusselt, Reynolds and Prandtl number relation is a non-dimensional heat transfer parameter based upon the Reynolds analogy.

In figure 5.17, a non-dimensional heat transfer parameter is plotted versus X_{tt} for upward flow. There are some distinct trends in the plots. First, the non-dimensional heat transfer parameter is inversely proportional to X_{tt}. Next, at an $X_{tt} \approx 0.3$, there is a discontinuity with a change in slope of the inverse proportionality. Finally, at the lowest mass flux tested, G = 37 $\mathrm{klb_m/ft^2}$-hr (50 $\mathrm{kg/m^2}$-s), these data points have different slopes relative to the higher mass fluxes. Table 5.1 shows the curve fits for the various trends for the upward flow configuration.

For the downward flow configuration, figure 5.18 shows the relation between the non-dimensional heat transfer parameter and X_{tt}. As in the upward flow configuration, there is an inverse relation between the non-dimensional heat transfer parameter and X_{tt}. Again, there is a discontinuity at $X_{tt} \approx 0.3$, as well as a change in slope in the decreasing function. An interesting trend for this downward flow configuration is that the lowest mass flux data, G = 37 klb_m/ft^2-hr (50 kg/m^2-s), is not discernible from the other mass flux tests. Table 5.2 shows the fitted equations for the two distinct trends found in the downward flow configuration.

Upon further inspection of the trends presented in figures 5.17 and 5.18, the discontinuity at $X_{tt} \approx 0.3$ is a consistent characteristic of both flow configurations and all mass fluxes. At $X_{tt}<0.3$, for all the mass and heat fluxes, these tests represent the low quality tests $(x \approx 0.2)$. Once the quality increases, the non-dimensional heat transfer parameter shifts to another trend line. This behavior could be justified by a flow transition (possibly film flow to film-wispy flow) that causes the heat transfer characteristics to abruptly change at a certain quality. Also, this phenomenon is consistent with the boiling mechanism results since nucleate boiling is generally suppressed at higher qualities. When the nucleate boiling mechanism is suppressed, the heat transfer characteristics of the conditions are altered which may account for the shift in the trend line. Another interesting point is that at G = 37 klb_m/ft^2-hr (50 kg/m^2-s) for upward flow, the heat transfer trend deviates from the other data points. Again, there must be some kind of flow transition or other mechanism that causes this behavior to occur.

Once the data was compiled, it was compared with two of the correlations presented in the literature review. First, the experimental data is compared to Chen's [1966] upward flow correlation for round tubes. In the calculations for Chen's correlation, the hydraulic diameter of the test section was used when a flow diameter was required. Upon analysis of the correlated versus experimental results, the Chen correlation severely under predicts the experimental data, as shown in figure 5.19. This under prediction could be attributed to the correlation's inability to capture the non-circular geometry or obstructed flow effects. By examining the individual test runs, in

Appendix, it seems that Chen's correlation does not predict the heat transfer coefficients accurately at the higher qualities. But as the quality decreases, generally, the prediction error of Chen's correlation decreases, as shown in figure 5.23. The second correlation used for comparison is based upon Carey and Mandrusiak's [1989] work. This correlation is based upon upward, annular flow in a partially heated channel. In figure 5.22, Carey and Mandrusiak's correlation under predicts a majority of the data points. By observing the deviation versus quality plot in figure 5.24, there is a wide spread of error at the lower qualities which might be attributed to the purely convective boiling model used for this correlation.

Table 5.1 Fitted Equations for *Upward Flow.*

Conditions	Fit Equation	R^2
G = 37 klb_m/ft^2-hr (50 kg/m^2-s), $X_{tt}<0.3$	$\frac{Nu}{Re_l^{0.7} Pr_l^{0.3}} = 0.3031 \cdot X_{tt}^{-0.8099}$	0.956
G = 37 klb_m/ft^2-hr (50 kg/m^2-s), $X_{tt}>0.3$	$\frac{Nu}{Re_l^{0.7} Pr_l^{0.3}} = 0.4775 \cdot X_{tt}^{-0.5941}$	0.924
All Other Tested Mass Fluxes, $X_{tt}<0.3$	$\frac{Nu}{Re_l^{0.7} Pr_l^{0.3}} = 0.2177 \cdot X_{tt}^{-0.8748}$	0.986
All Other Tested Mass Fluxes, $X_{tt}>0.3$	$\frac{Nu}{Re_l^{0.7} Pr_l^{0.3}} = 0.2512 \cdot X_{tt}^{-1.0403}$	0.862

Table 5.2 Fitted Equations for *Downward Flow.*

Conditions	Fit Equation	R^2
All Tested Mass Fluxes, $X_{tt}<0.3$	$\frac{Nu}{Re_l^{0.7} Pr_l^{0.3}} = 0.2175 \cdot X_{tt}^{-0.8154}$	0.9348
All Tested Mass Fluxes, $X_{tt}>0.3$	$\frac{Nu}{Re_l^{0.7} Pr_l^{0.3}} = 0.1776 \cdot X_{tt}^{-1.4007}$	0.9149

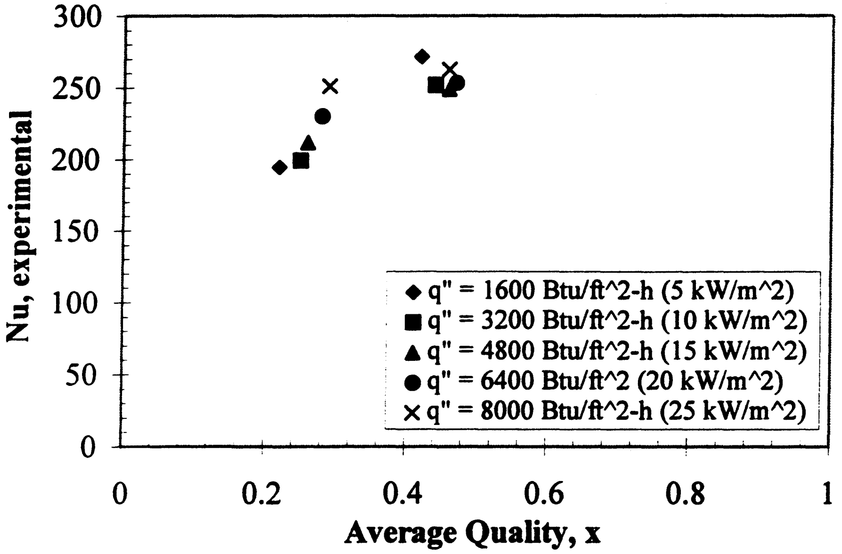

Figure 5.1 Experimental Nusselt number versus average quality for *upward* flow at G = 220 klb$_m$/ft^2-hr (300 kg/m^2-s)

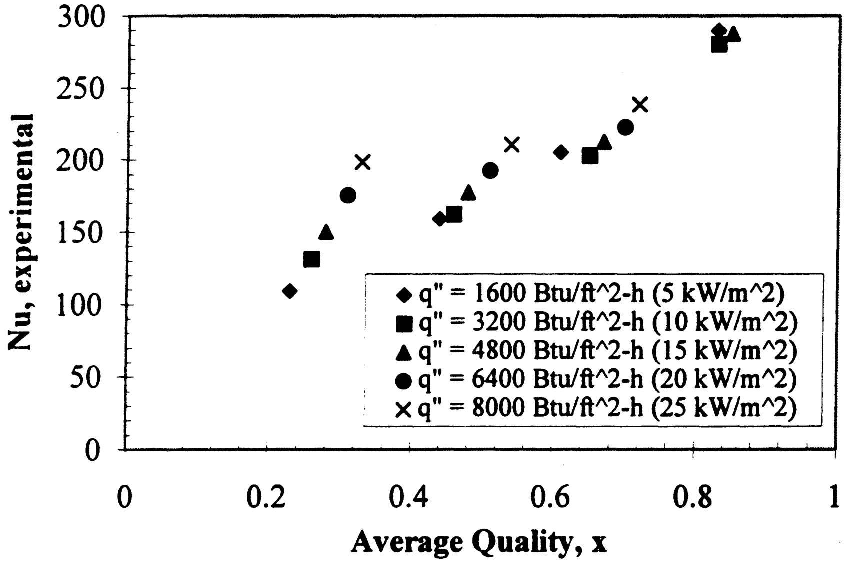

Figure 5.2 Experimental Nusselt number versus average quality for *upward* flow at G = 110 klb$_m$/ft^2-hr (150 kg/m^2-s)

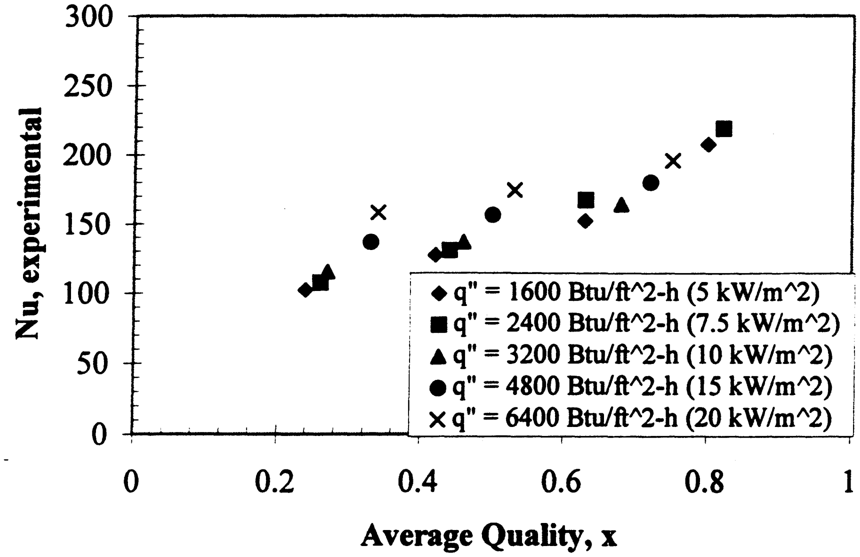

Figure 5.3 Experimental Nusselt number versus average quality for *upward* flow at $G = 75$ klb$_m$/ft^2-hr (100 kg/m^2-s)

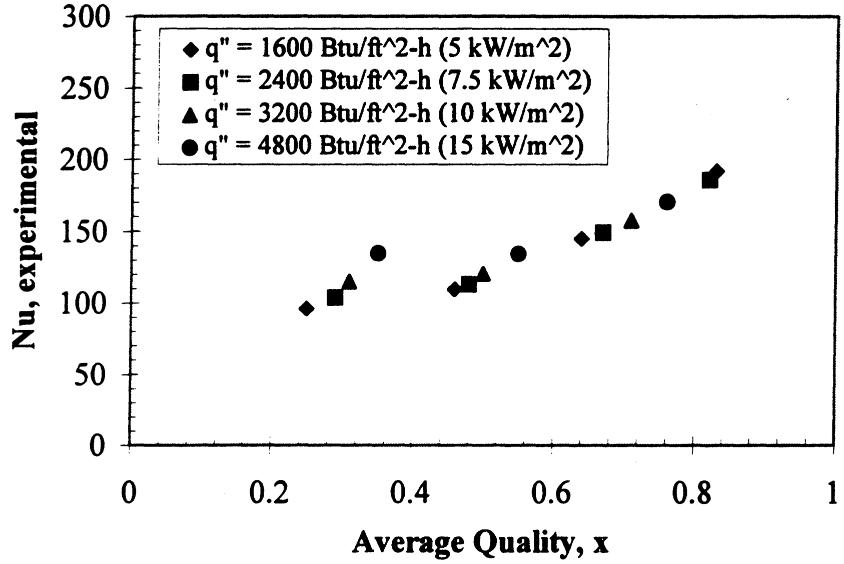

Figure 5.4 Experimental Nusselt number versus average quality for *upward* flow at $G = 56$ klb$_m$/ft^2-hr (75 kg/m^2-s)

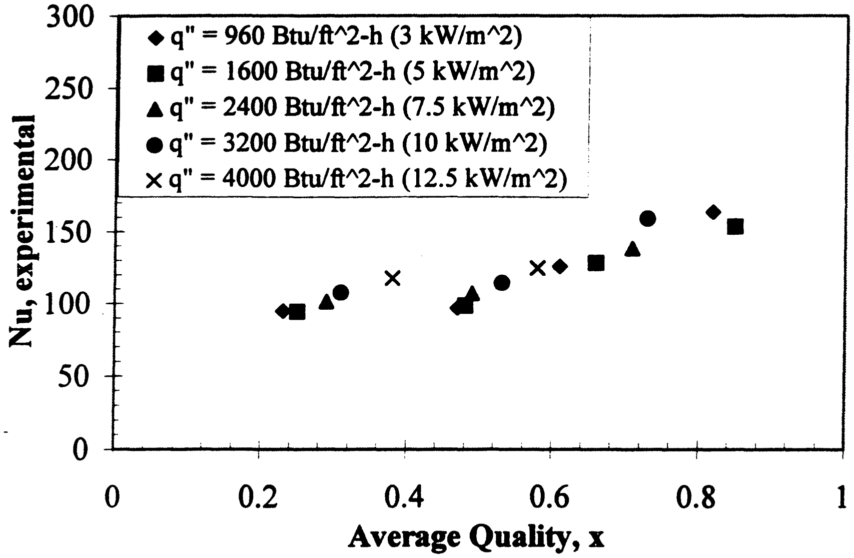

Figure 5.5 Experimental Nusselt number versus average quality for *upward* flow at G = 37 klb_m/ft^2-hr (50 kg/m^2-s)

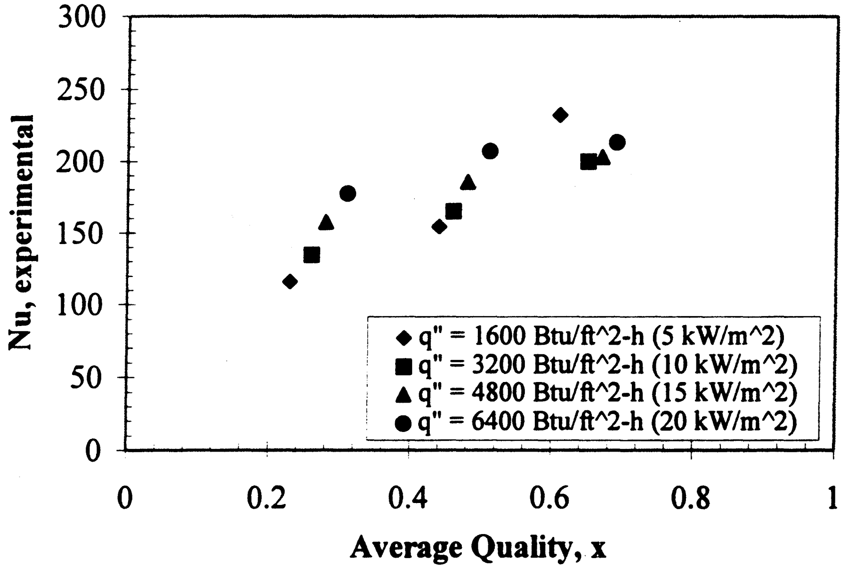

Figure 5.6 Experimental Nusselt number versus average quality for *downward* flow at G = 110 klb_m/ft^2-hr (150 kg/m^2-s)

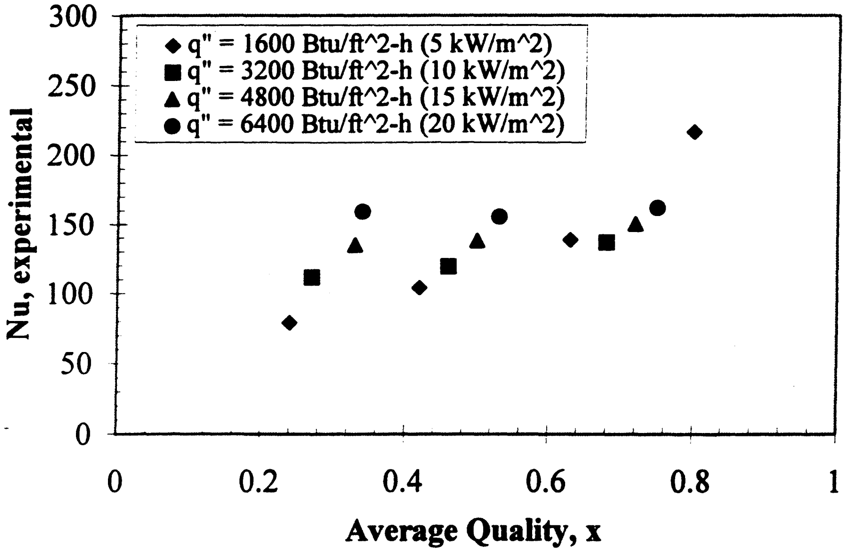

Figure 5.7 Experimental Nusselt number versus average quality for *downward* flow at G = 75 klb_m/ft^2-hr (100 kg/m^2-s)

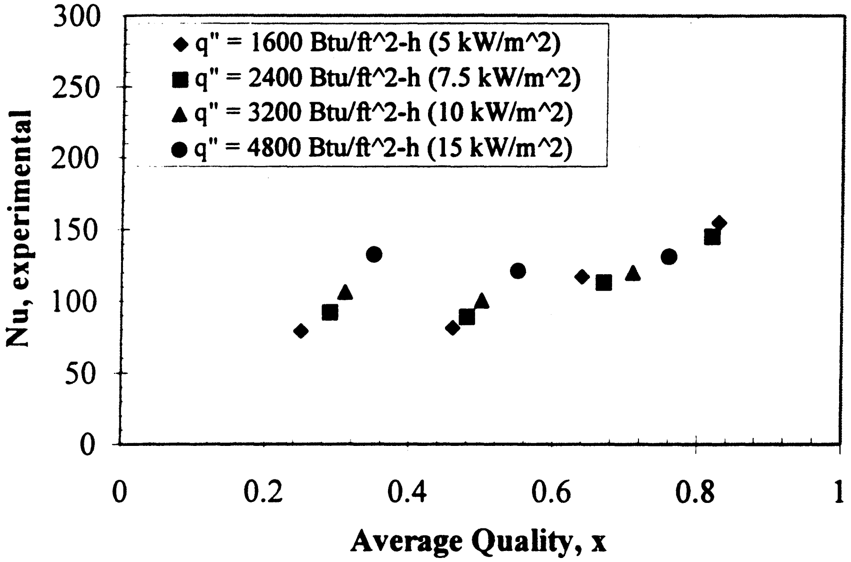

Figure 5.8 Experimental Nusselt number versus average quality for *downward* flow at G = 56 klb_m/ft^2-hr (75 kg/m^2-s)

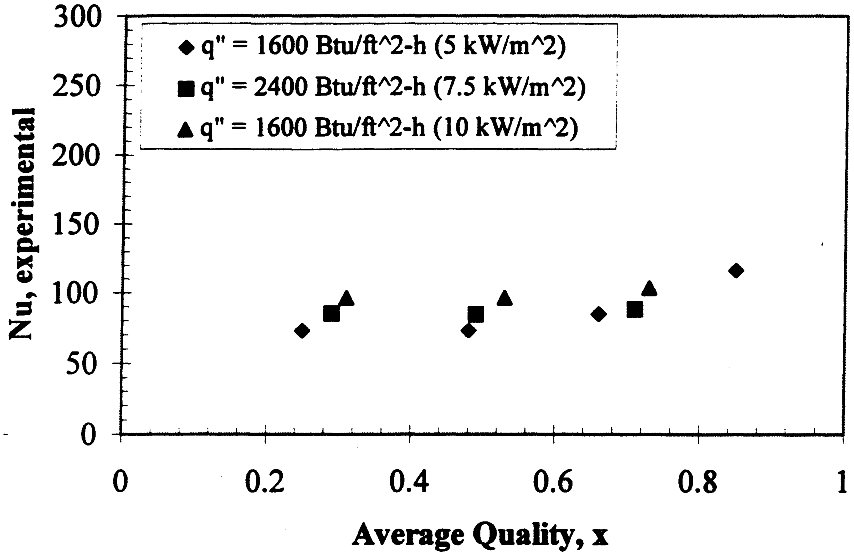

Figure 5.9 Experimental Nusselt number versus average quality for *downward* flow at G = 37 klb_m/ft^2-hr (50 kg/m^2-s)

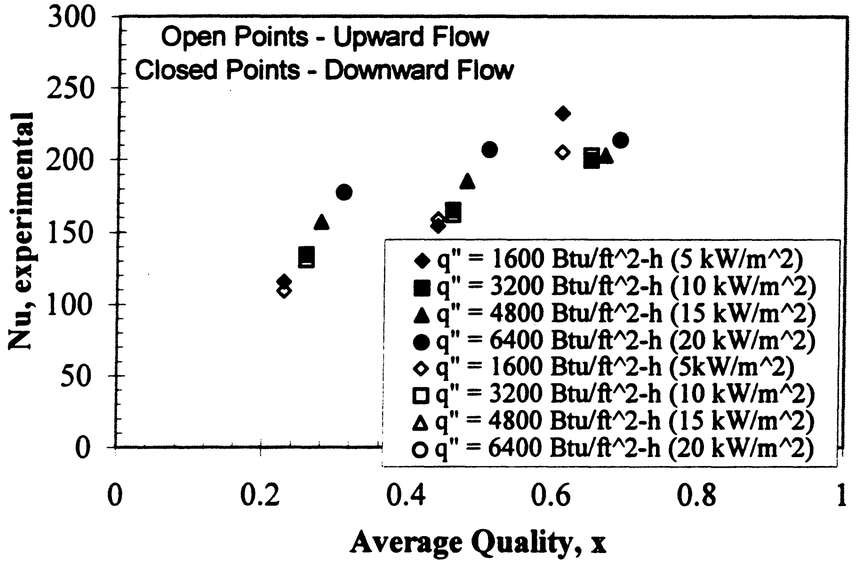

Figure 5.10 Experimental Nusselt number versus average quality, comparison of upward and downward flow at G = 110 klb_m/ft^2-hr (150 kg/m^2-s)

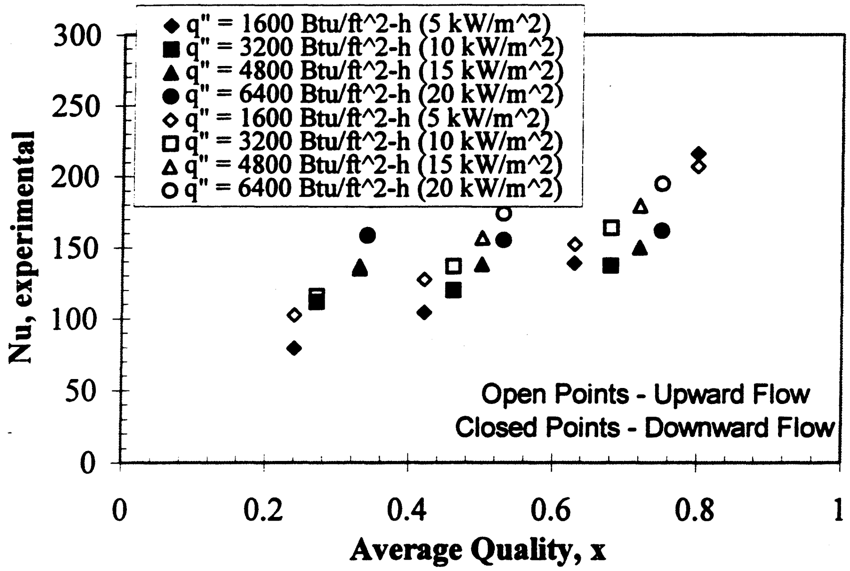

Figure 5.11 Experimental Nusselt number versus average quality, comparison of upward and downward flow at G = 75 klb$_m$/ft^2-hr (100 kg/m^2-s)

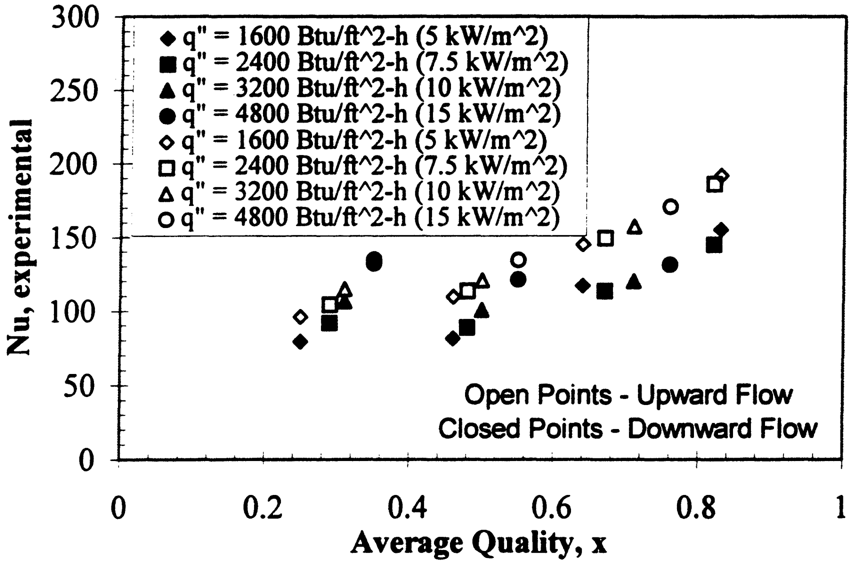

Figure 5.12 Experimental Nusselt number versus average quality, comparison of upward and downward flow at G = 56 klb$_m$/ft^2-hr (75 kg/m^2-s)

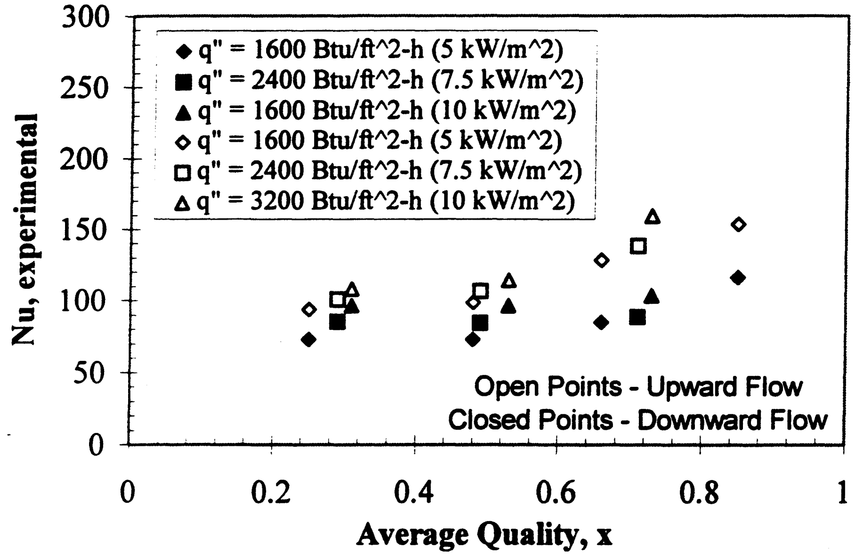

Figure 5.13 Experimental Nusselt number versus average quality, comparison of upward and downward flow at G = 37 klb$_m$/ft^2-hr (50 kg/m^2-s)

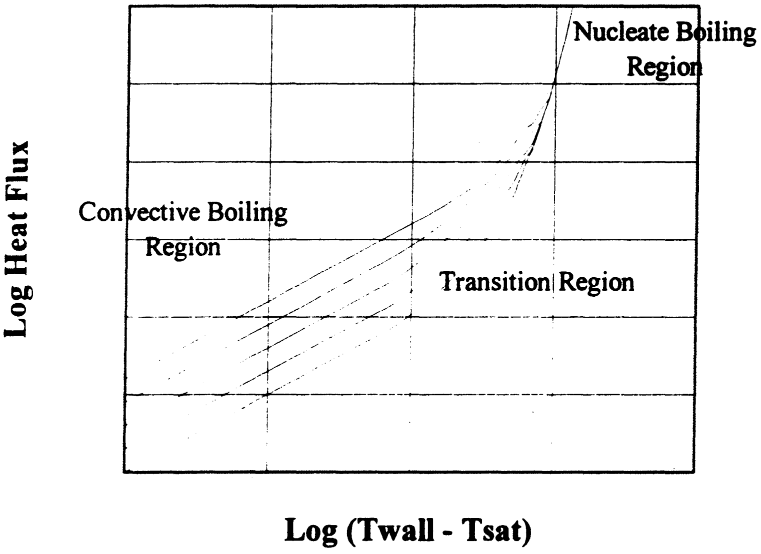

Figure 5.14 Schematic of Traditional Boiling Curves

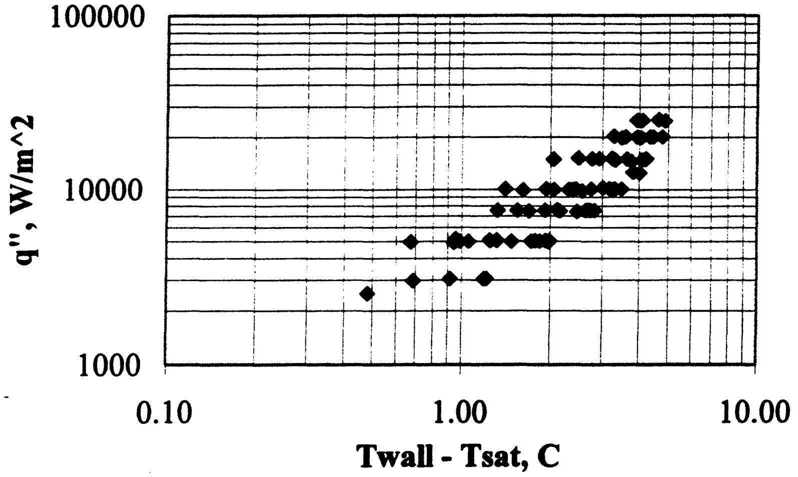

Figure 5.15 Heat flux versus $\Delta T_s = \left(T_w - T_{sat}\right)$ for *upward* flow.

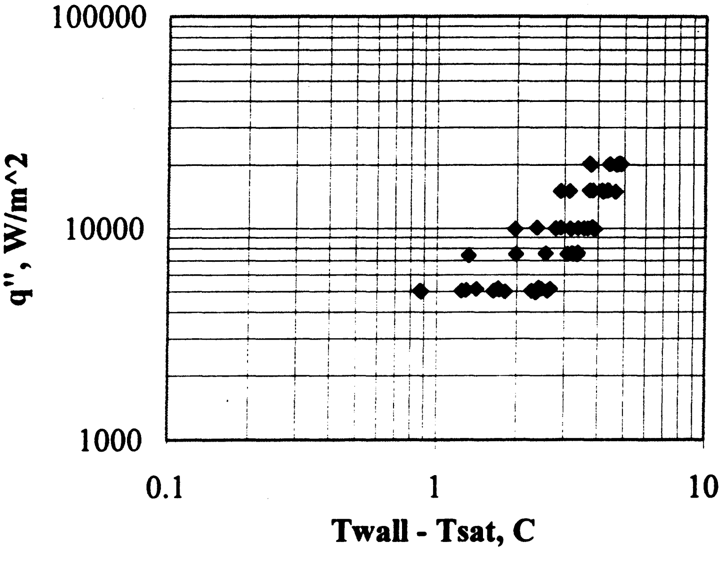

Figure 5.16 Heat flux versus $\Delta T_s = \left(T_w - T_{sat}\right)$ for *downward* flow.

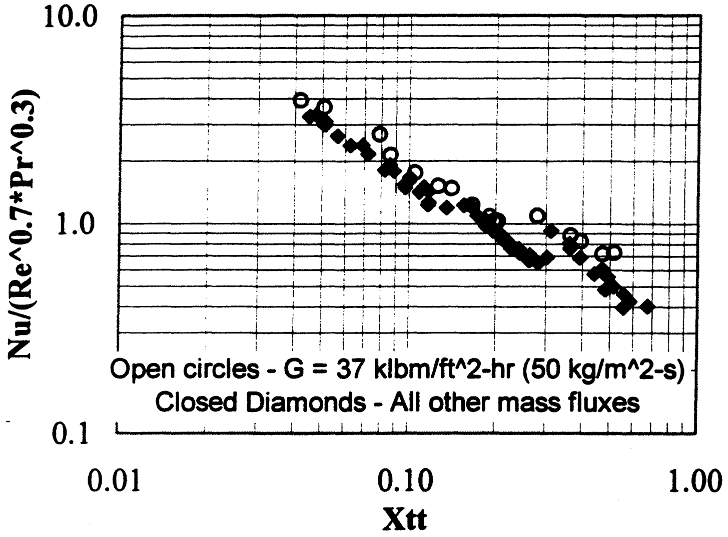

Figure 5.17 Nu/($Re^{0.7}Pr^{0.3}$) vs. X_{tt} for *upward* flow.

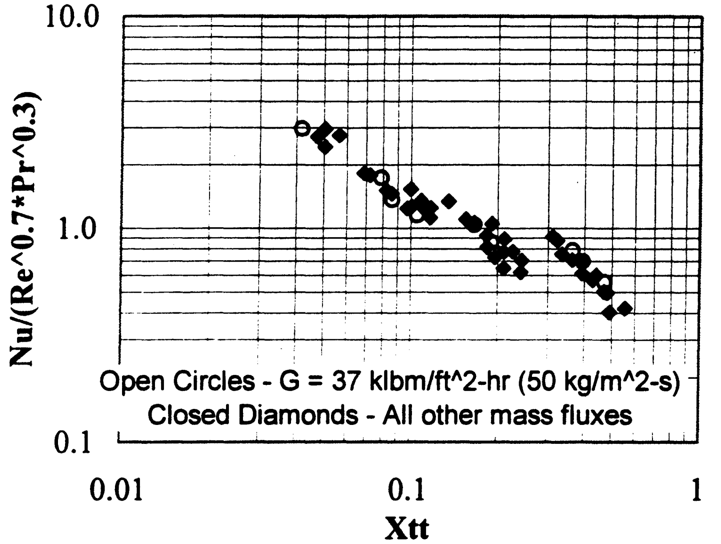

Figure 5.18 Nu/($Re^{0.7}Pr^{0.3}$) vs. X_{tt} for *downward* flow.

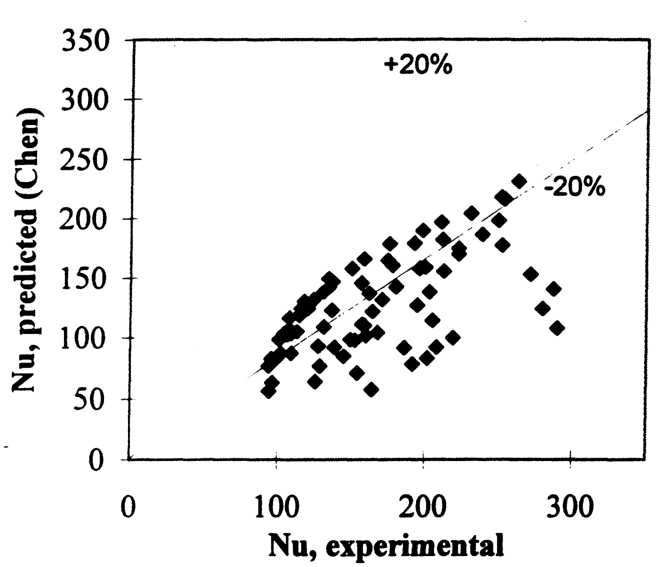

Figure 5.19 Experimental Nusselt number versus predicted Nusselt number for Chen correlation

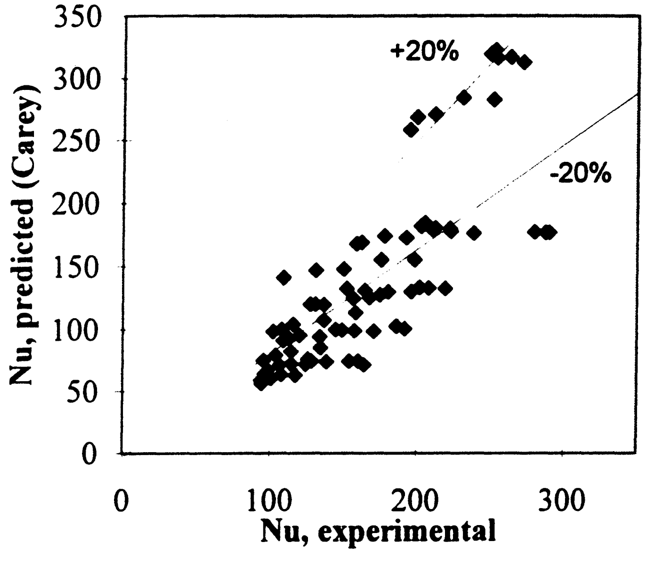

Figure 5.20 Experimental Nusselt number versus predicted Nusselt number for Carey correlation

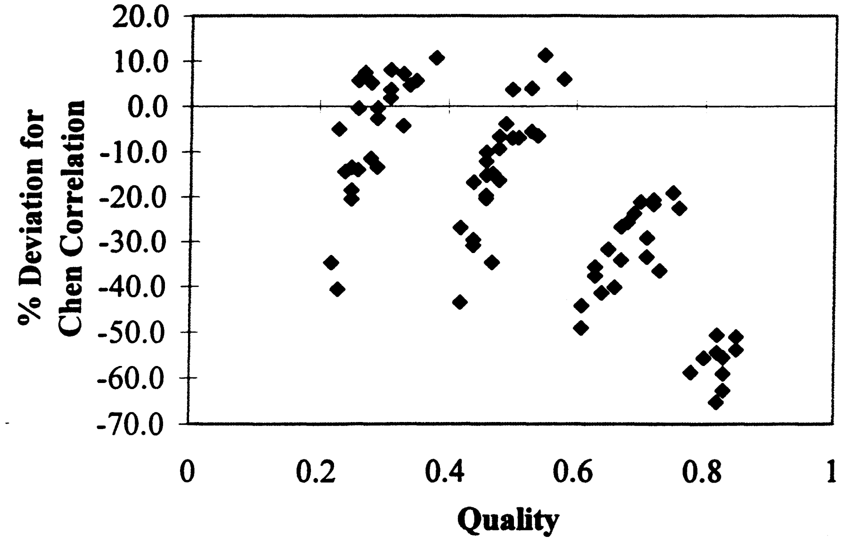

Figure 5.21 Percent Deviation for Chen's Correlation relative to experimental data versus quality

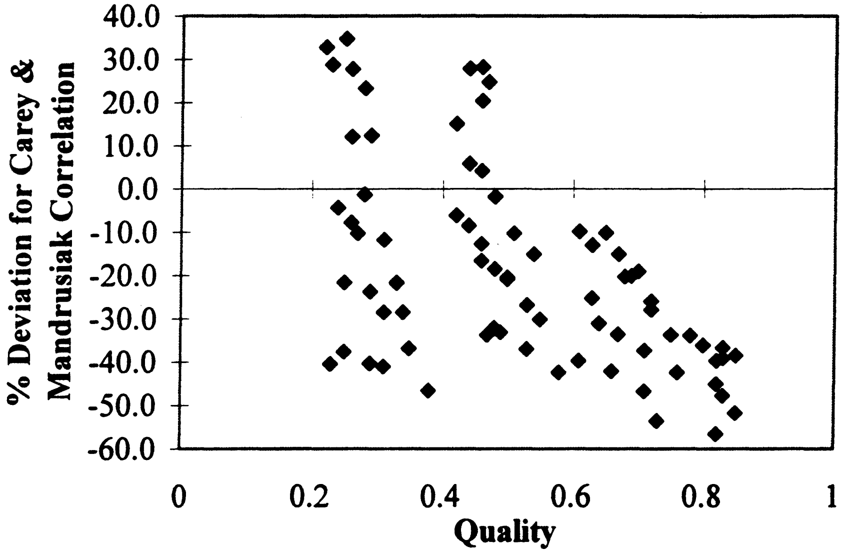

Figure 5.22 Percent Deviation for Carey and Mandrusiak's Correlation relative to experimental data versus quality

CHAPTER 6
Conclusion

The goal of this investigation was to study the heat transfer characteristics of evaporative two-phase flows, particularly in a non-circular geometry with flow obstructions that is configured vertically. In this study, experimental data were collected and analyzed in order to gain a better understanding of boiling heat transfer in variable non-circular geometries. The following sections will provide the conclusions from this work.

In this variable non-circular geometry, Nusselt number varies with both quality and heat flux. As quality increases, Nusselt number increases for all mass fluxes which indicates the presence of convective boiling. For the lowest qualities, a heat flux dependence is observed which is indicative of nucleate boiling. In all of the experiments that were performed, a film flow regime is believed to dominate.

Both upward and downward flow configurations were studied. For high mass fluxes, upward and downward flow produced similar results. As mass flux decreased, the upward flow configuration provided enhanced heat transfer relative to the downward flow configuration, particularly at the higher qualities. Also, the downward flow heat transfer results show a greater heat flux dependence when compared to the upward flow configuration. In general, upward flow at the lower mass fluxes suppressed nucleate boiling and convective boiling was enhanced when comparing heat transfer performance to downward flow.

Empirical correlations were developed because two correlations presented in the literature give unsatisfactory results. Chen's correlation [1966] for round tubes severely under predicts the experimental data. Apparently, the vertical round tube correlation does not capture the non-circular and obstructed flow effects. The experimental data was also compared to Carey and Mandrusiak's [1989] upward channel correlation which also under predicts a majority of the data. Considerably more data on different geometries is needed to develop generalized correlations for plate type evaporators.

REFERENCES

Bennett, D.L., and Chen, J.C., "Forced convective boiling in vertical tubes for saturated pure components and binary mixtures," AICHE Journal, vol. 26, no. 3, 1980

Carey, V.P., *Liquid-vapor Phase Change Phenomena*, Hemisphere, New York, 1992

Carey, V.P., and Mandrusiak, G.D., "Annular film-flow boiling of liquids in a partially heated, vertical channel with offset strip fins," International Journal of Heat and Mass Transfer, vol. 29, no.6, pp. 927-939, 1986

Chen, J.C., "Correlation for boiling heat transfer to saturated fluids in convective flow," Industrial Engineering Chemical Process Design and Development, vol. 5, no. 3, pp.322-339, 1966

Chopard, F., Marvillet, Ch., and Pantaloni, J., "Assessment of heat transfer performance of rectangular channel geometries; Implications on refrigerant evaporator and condenser design," ICHEME Symposium Series, no. 129, 1994

Cohen, M., and Carey, V.P., "A comparison of the flow boiling performance characteristics of partially-heated cross-ribbed channels with different rib geometries," International Journal of Heat and Mass Transfer, vol. 32, no.12, pp. 2459-2474, 1989

Forster, H.K., and Zuber, N., "Dynamics of vapor bubbles and boiling heat transfer," AICHME Journal, vol. 1, pp. 531-535, 1955

Hewitt, G.F., and Roberts, D.N., "Studies of two-phase flow patterns by simultaneous X-ray and flash photography," AERE-M 2159, Her Majesty's Stationery Office, London, 1969

Kandlikar, S.G., "A general correlation for saturated two-phase flow boiling heat transfer inside horizontal and vertical tubes," Journal of Heat Transfer, vol. 112, pp.219-228, 1989

Kaska, K.E., and Wambsganss, M.W., "Flow visualization of microscale thermal mechanics of boiling in small channels," Argonne National Laboratory, Energy Technology Division, Contract W-31-109-Eng-38, 1995

Moffat, R.J., "Describing the uncertainties in experimental results," Experimental Thermal and Fluid Science 1, 3-17, 1988

Ohara, T., Yamamoto, T., and Fujita, H., "Evaporative heat transfer and pressure drop in a rib-roughened flat channel (Effects of height and spacing of repeated transverse rib roughness)," ASME/JSME Thermal Engineering Proceedings, vol. 4, 1991

Robertson, J.M., "Boiling heat transfer with liquid nitrogen in brazed-aluminum plate-fin exchangers," AICHE Symposium Series, no. 189, vol. 75, 1979

Robertson, J.M., "Boiling heat transfer with freon 11 (R11) in brazed aluminum, plate-fin heat exchangers," Journal of Heat Transfer, vol. 105, 1983

Robertson, J.M., "The prediction of convective boiling coefficients in serrated plate-fin passages using an interrupted liquid-flim flow model," ASME, HTD, vol. 34, 1984

Shah, M.M., "Chart correlations for saturated boiling heat transfer: Equations and further study," ASHRAE Transactions, vol. 88, part 1, pp. 185-196, 1982

Steiner, D., and Taborek, J., "Flow boiling heat transfer in vertical tubes correlated by an asymptotic model," Heat Transfer Engineering, vol. 13, no.2, 1992

Tran, T.N., Wambsganss, M.W., and France, D.M., "Boiling heat transfer with three fluids in small circular and rectangular channels," Argonne National Laboratory, Energy Technology Division, Contract W-31-109-Eng-38, 1995

Wambsganss, M.W., Jendrzejczyk, J.A., and France, D.M., "Two-phase flow and pressure drop in flow passages of compact heat exchangers," SAE Technical Paper Series, 920550, 1992

Wattelet, J.P., "Design, building, and baseline testing of an apparatus used to measure evaporation characteristics of ozone-safe refrigerants," M.S. thesis, University of Illinois at Urbana-Champaign, 1990

Wattelet, J.P., "Heat transfer flow regimes of refrigerants in a horizontal-tube evaporator," Ph.D. Thesis, University of Illinois at Urbana-Champaign, 1994

Xu, X., and Carey, V.P., "An experimental study of the effects of channel orientation on convective boiling in a partially cross-ribbed channel," International Journal of Heat and Mass Transfer, vol. 30, pp. 2397-2397, 1987

APPENDIX

All of the heat transfer data collected in this study are listed in Appendix A. The headings and units for the following tables are as follows: T_{sat}, saturation temperature °C; G, refrigerant mass flux (kg/m^2-s); q", test section heat flux (kW/m^2); x_{in}, inlet quality; x_{ave}, average quality; rhol/rhov, density ratio (liquid/vapor); muv/mul, viscosity ratio (vapor/liquid); ho1, experimental heat transfer coefficient for upward and downward flow (W/m^2-°C); Nu, Nusselt Number for upward and downward flow; dh computed uncertainty in the experimental heat transfer coefficient; dh/h computed uncertainty divided by experimental heat transfer coefficient.

							Upward		**Downward**			
Tsat	q"	G	x in	x ave	rhol/rhov	muv/mul	hol	Nul-u	hol	Nu-d	dh	dh/h
20	5	304	40	42	44.47	0.0564	6612	272			2567	0.39
20	9.9	311	41	44	44.41	0.0564	6136	252			1251	0.20
20	15.1	304	41	46	44.52	0.0564	6068	249			935	0.15
20	20.3	300	41	47	44.54	0.0564	6175	254			833	0.13
20	25	301	39	46	44.35	0.0565	6393	263			810	0.13
20	5	304	20	22	44.39	0.0564	4735	195			1361	0.29
20	10	303	22	25	44.38	0.0565	4857	200			837	0.17
20	15	301	22	26	44.44	0.0564	5152	212			733	0.14
20	20	309	22	28	44.31	0.0565	5608	231			733	0.13
20	25	304	22	29	44.34	0.0565	6117	252			764	0.12
10	5	152	81	83	62.49	0.0484	7485	290			3263	0.44
10	10	152	78	83	62.42	0.0485	7230	280			1659	0.23
10	15	152	77	85	62.32	0.0485	7420	288			1294	0.17
10	5	158	59	61	62.55	0.0484	5293	205	5996	232	1678	0.32
10	10	155	59	65	62.09	0.0486	5228	203	5155	200	945	0.18
10	15	153	59	67	62.36	0.0485	5481	212	5241	203	804	0.15
10	20	152	59	69	62.85	0.0483	5754	223	5517	213	760	0.13
10	20	150	59	70	62.11	0.0486	5735	222			756	0.13
10	25	150	58	72	62.55	0.0484	6155	238			770	0.13
10	5	152	41	44	62.36	0.0485	4103	159	3983	154	1044	0.25
10	10	151	40	46	62.51	0.0484	4186	162	4264	165	660	0.16
10	15	155	40	48	62.25	0.0485	4579	177	4785	185	619	0.14
10	20	151	41	51	62.29	0.0485	4969	193	5341	207	624	0.13
10	25	155	41	54	62.38	0.0485	5436	211			657	0.12
10	5	155	21	23	62.36	0.0485	2825	109	2984	116	539	0.19
10	10	156	20	26	62.36	0.0485	3382	131	3474	135	478	0.14
10	15	153	20	28	62.52	0.0484	3877	150	4058	157	493	0.13
10	20	156	20	31	62.19	0.0485	4530	176	4584	178	553	0.12
10	25	152	20	33	62.21	0.0485	5112	198			608	0.12

Tsat	q"	G	x in	x ave	rhol/rhov	muv/mul	Upward		Downward		dh	dh/h
							hol	Nul-u	hol	Nu-d		
5	5.2	107	77	80	74.30	0.0447	5514	208	5748	217	1750	0.32
5	7.6	106	77	82	74.20	0.0448	5815	219	5718	215	1396	0.24
5	5	108	59	63	74.41	0.0447	4047	152	3689	139	1018	0.25
5	7.5	101	57	63	73.99	0.0448	4442	167			876	0.20
5	10	105	60	68	73.90	0.0448	4358	164	3650	138	703	0.16
5	15	104	60	72	74.13	0.0448	4778	180	3998	151	657	0.14
5	20	104	60	75	74.32	0.0447	5199	196	4314	163	662	0.13
5	5	106	38	42	74.24	0.0448	3388	128	2767	104	739	0.22
5	7.5	105	38	44	74.24	0.0448	3485	131			584	0.17
5	10	103	38	46	74.56	0.0447	3633	137	3179	120	531	0.15
5	15	105	39	50	74.24	0.0448	4159	157	3670	138	542	0.13
5	20	107	38	53	74.70	0.0446	4632	174	4130	155	569	0.12
5	5	103	20	24	74.16	0.0448	2720	103	2105	79	505	0.19
5	7.5	101	20	26	74.47	0.0447	2866	108			430	0.15
5	10	106	19	27	74.28	0.0447	3073	116	2970	112	417	0.14
5	15	101	21	33	74.24	0.0448	3635	137	3585	135	453	0.12
5	20	106	19	34	74.35	0.0447	4207	158	4224	159	504	0.12
5	5	77	78	83	74.65	0.0446	5093	192	4114	155	1560	0.31
5	7.6	79	74	82	74.36	0.0447	4938	186	3853	145	1043	0.21
5	5	78	59	64	74.25	0.0448	3842	145	3108	117	926	0.24
5	7.6	77	59	67	74.32	0.0447	3962	149	3007	113	715	0.18
5	10	76	60	71	74.09	0.0448	4175	157	3182	120	657	0.16
5	15	75	60	76	74.28	0.0447	4533	171	3483	131	610	0.13
5	5	76	41	46	74.18	0.0448	2901	109	2163	82	564	0.19
5	7.5	76	40	48	74.41	0.0447	3007	113	2365	89	463	0.15
5	10	78	39	50	73.90	0.0448	3194	120	2666	101	440	0.14
5	15	75	39	55	74.31	0.0447	3570	134	3221	121	442	0.12
5	5	75	20	25	74.24	0.0448	2542	96	2098	79	451	0.18
5	7.6	75	21	29	74.27	0.0447	2762	104	2445	92	404	0.15
5	10	77	21	31	74.35	0.0447	3045	115	2823	106	411	0.14
5	15	77	19	35	73.96	0.0448	3579	135	3511	132	444	0.12

							Upward		**Downward**			
Tsat	q"	G	x in	x ave	rhol/rhov	muv/mul	hol	Nul-u	hol	Nu-d	dh	dh/h
5	3	51	77	82	74.26	0.0447	4358	164			1847	0.42
5	5	53	77	85	74.52	0.0447	4093	154	3102	117	1039	0.25
5	3	58	57	61	74.07	0.0448	3341	126		0	1108	0.33
5	5	55	58	66	73.92	0.0448	3413	129	2252	85	748	0.22
5	7.6	54	60	71	73.83	0.0449	3681	139	2355	89	633	0.17
5	9.8	54	59	73	74.38	0.0447	4247	160	2750	104	683	0.16
5	3.1	51	42	47	74.25	0.0447	2568	97			658	0.26
5	5	53	40	48	74.24	0.0448	2619	99	1940	73	474	0.18
5	7.6	56	38	49	73.98	0.0448	2834	107	2239	84	420	0.15
5	10	56	38	53	74.01	0.0448	3038	115	2560	97	410	0.13
5	12.6	54	39	58	73.72	0.0449	3301	125			422	0.13
5	3	56	19	23	74.09	0.0448	2509	95			648	0.26
5	5	57	18	25	74.21	0.0448	2497	94	1940	73	438	0.18
5	7.6	56	18	29	74.15	0.0448	2685	101	2269	86	387	0.14
5	10	58	17	31	74.25	0.0448	2870	108	2566	97	379	0.13
5	12.5	53	19	38	74.22	0.0448	3126	118			393	0.13